Znf598-mediated Rps10/eS10 ubiquitination contributes to the ribosome ubiquitination dynamics during zebrafish development

NOZOMI UGAJIN,[1] KOSHI IMAMI,[2,3] HIRAKU TAKADA,[1] YASUSHI ISHIHAMA,[3] SHINOBU CHIBA,[1] and YUICHIRO MISHIMA[1]

[1]Department of Frontier Life Sciences, Faculty of Life Sciences, Kyoto Sangyo University, Kita-ku, Kyoto 603-8555, Japan
[2]RIKEN Center for Integrative Medical Sciences, Tsurumi-ku, Yokohama, Kanagawa 230-0045, Japan
[3]Graduate School of Pharmaceutical Sciences, Kyoto University, Sakyo-ku, Kyoto 606-8501, Japan

ABSTRACT

The ribosome is a translational apparatus that comprises about 80 ribosomal proteins and four rRNAs. Recent studies reported that ribosome ubiquitination is crucial for translational regulation and ribosome-associated quality control (RQC). However, little is known about the dynamics of ribosome ubiquitination under complex biological processes of multicellular organisms. To explore ribosome ubiquitination during animal development, we generated a zebrafish strain that expresses a FLAG-tagged ribosomal protein Rpl36/eL36 from its endogenous locus. We examined ribosome ubiquitination during zebrafish development by combining affinity purification of ribosomes from *rpl36*-FLAG zebrafish embryos with immunoblotting analysis. Our findings showed that the ubiquitination of ribosomal proteins dynamically changed as development proceeded. We also showed that during zebrafish development, the ribosome was ubiquitinated by Znf598, an E3 ubiquitin ligase that activates RQC. Ribosomal protein Rps10/eS10 was found to be a key ubiquitinated protein during development. Furthermore, we showed that Rps10/eS10 ubiquitination-site mutations reduced the overall ubiquitination pattern of the ribosome. These results demonstrate the complexity and dynamics of ribosome ubiquitination during zebrafish development.

Keywords: development; ribosome; ubiquitination; zebrafish

INTRODUCTION

The ribosome is a large ribonucleoprotein complex that plays a central role in translation in all living organisms. The eukaryotic 80S ribosome consists of about 80 ribosomal proteins and four ribosomal RNA (rRNA) molecules organized into a large 60S subunit and a small 40S subunit (Bashan and Yonath 2008; De La Cruz et al. 2015). While there are some species-specific differences, these core ribosomal components are essential constituents for the ribosome to function as a translation apparatus. In addition, posttranslational modifications on ribosomal proteins modulate the functionality of the ribosome (Xue and Barna 2012; Simsek and Barna 2017; Dalla Venezia et al. 2019; Emmott et al. 2019; Li and Wang 2020). Ribosomal proteins have been reported to undergo a range of posttranslational modifications, including phosphorylation (Martin et al. 2014; Imami et al. 2018), ubiquitination (Spence et al. 2000; Higgins et al. 2015; Silva et al. 2015; Back et al. 2019; Matsuki et al. 2020), methylation (Małecki et al. 2021; Matsuura-Suzuki et al. 2022), acetylation (Zhang et al. 2022), and UFMylation (Walczak et al. 2019; Wang et al. 2020). Some of these modifications are introduced to the ribosome in response to various stimuli, and affect multiple aspects of translation, such as translation efficiency (Takehara et al. 2021; Matsuura-Suzuki et al. 2022) and selectivity (Imami et al. 2018; Matsuki et al. 2020; Zhang et al. 2022). Hence, ribosomes in a given cell or organism are subjected to dynamic changes in their modification status to adapt to diverse translational demands.

Recent studies have emphasized the significance of ribosome ubiquitination in the context of translating ribosome quality control. When a ribosome slows aberrantly during translation, it collides with the trailing ribosome to form a

Corresponding author: mishima@cc.kyoto-su.ac.jp
Article is online at http://www.rnajournal.org/cgi/doi/10.1261/rna.079633.123.

specific structure called a disome (Juszkiewicz et al. 2018; Ikeuchi et al. 2019). Ribosome collision and disome formation trigger the ribosome-associated quality control (RQC) pathway, which dissociates stalled ribosomes into subunits and degrades nascent polypeptides (Joazeiro 2017, 2019; Inada 2020). The site-specific ubiquitination of the 40S ribosomal proteins Rps10/eS10 and Rps20/uS10 in the disome initiates the RQC pathway (Garzia et al. 2017; Juszkiewicz and Hegde 2017; Matsuo et al. 2017; Sundaramoorthy et al. 2017). These reactions are catalyzed by an E3 ubiquitin ligase ZNF598 (Hel2 in yeast), which recognizes the disome structure by an unknown mechanism (Garzia et al. 2017; Juszkiewicz and Hegde 2017; Matsuo et al. 2017; Sundaramoorthy et al. 2017; Juszkiewicz et al. 2018). Ubiquitinated forms of Rps10/eS10 and/or Rps20/uS10 are recognized by the ASC-1 complex (also known as RQT complex in yeast), in which an ATP-dependent RNA helicase ASCC3 (Slh1/Rqt2 in yeast) dissociates the stalled ribosome into subunits (Matsuo et al. 2017, 2020; Sitron et al. 2017; Juszkiewicz et al. 2020b; Narita et al. 2022). Another E3 ubiquitin ligase, Ltn1, polyubiquitinates a nascent polypeptide in the split 60S subunit, which is then degraded by the proteasome (Bengtson and Joazeiro 2010; Brandman et al. 2012; Shao and Hegde 2014). The Rps10/eS10 and/or Rps20/uS10 ubiquitination also promote endonucleolytic cleavage of the mRNA with the stalled ribosome, known as no-go decay (NGD) (D'Orazio et al. 2019; Ikeuchi et al. 2019; Glover et al. 2020). In addition to the RQC and NGD pathways, an E3 ubiquitin ligase called RNF10 (Mag2 in yeast) ubiquitinates the 40S ribosomal proteins Rps2/uS5 and Rps3/uS3 in response to decoding and initiation/elongation abnormalities. This results in the degradation of 40S subunits (Sugiyama et al. 2019; Garzia et al. 2021; Li et al. 2022). Monoubiquitination of Rps3/uS3 by Mag2 is followed by polyubiquitination by Fap1, Hel2, and Rsp5, leading to 18S nonfunctional rRNA decay (18S NRD) (Sugiyama et al. 2019; Li et al. 2022). Overall, these ribosome ubiquitination pathways maintain cellular proteostasis and protect the eukaryotic translation system against a variety of translational issues.

Ribosome ubiquitination is not limited to the quality control system. Rather, several studies revealed that ribosome ubiquitination is linked to a wide range of biological activities. In yeast, at least 37 ribosomal proteins are ubiquitinated in response to oxidative stress (Back et al. 2019). Furthermore, some site-specific ribosome ubiquitinations are required for cells to survive under ER stress (Higgins et al. 2015). Another example is the ubiquitination of the ribosomal protein Rpl28/uL15 during the S phase of the cell cycle (Spence et al. 2000). The ubiquitination state of the ribosome provides a clue to understanding translational regulation in several biological processes. However, little is known about the dynamics of ribosome ubiquitination during the life cycle of multicellular animals.

Biochemical analysis of ribosomes is often challenging in multicellular organisms, as samples from multiple tissues or developmental time points need to be processed in parallel. Ribosomes are often purified by sucrose gradient centrifugation (Johannes et al. 1999; Reschke et al. 2013). Although effective, this method necessitates long experimental durations and substantial quantities of biological materials, and changing the purifying conditions is challenging. An alternate method uses affinity purified ribosomes with a tagged ribosomal protein that is expressed either exogenously or endogenously (Inada et al. 2002; Sanz et al. 2009; Tryon et al. 2013; Shi et al. 2017; Simsek et al. 2017). This approach enables the purification of fully assembled 80S ribosomes in a relatively short duration and with a small amount of sample. In order to understand the complicated state of ribosome modifications in the life cycle of multicellular organisms, it will be beneficial to develop an affinity purification system of the ribosome in model animals.

Here, we used zebrafish as a model system to analyze the dynamics of ribosome ubiquitination during development. We generated a zebrafish strain expressing a FLAG-tagged ribosomal protein Rpl36/eL36 from the endogenous locus. We purified the ribosomes from zebrafish embryos and larvae using this strain, and we examined the temporal change of ribosome ubiquitination levels during zebrafish development. The present study reveals that Rps10/eS10 ubiquitination by Znf598 contributes to establishing a characteristic ubiquitination pattern during zebrafish development.

RESULTS

Establishment of a ribosome affinity purification system in zebrafish

To purify ribosomes from zebrafish embryos, we set up an affinity purification system with FLAG-tagged Rpl36/eL36 reported originally in mammalian cells (Simsek et al. 2017). We first verified the utility of this strategy in zebrafish embryos by injecting an mRNA encoding carboxy-terminally FLAG-tagged Rpl36/eL36 (Rpl36-FLAG). As expected, transiently expressed Rpl36-FLAG was incorporated into 80S ribosomes, enabling us to purify both the 40S and 60S subunits by FLAG-immunoprecipitation (Supplemental Fig. S1A–C). Then, using CRISPR–Cas9-mediated genome editing, we inserted a FLAG-tag sequence to the 3′ end of the endogenous zebrafish *rpl36* ORF in order to stabilize the expression of Rpl36-FLAG. As a result, we obtained a strain carrying an edited *rpl36* gene locus with the FLAG-tag sequence (Fig. 1A). The *rpl36*-FLAG allele was transmitted to offspring at the expected Mendelian ratio, suggesting that the inserted FLAG-tag sequence did not affect viability. Unless noticed, we used embryos obtained by crossing *rpl36*-FLAG heterozygous fish in this study (hereafter called *rpl36*-FLAG embryos). Fractionation

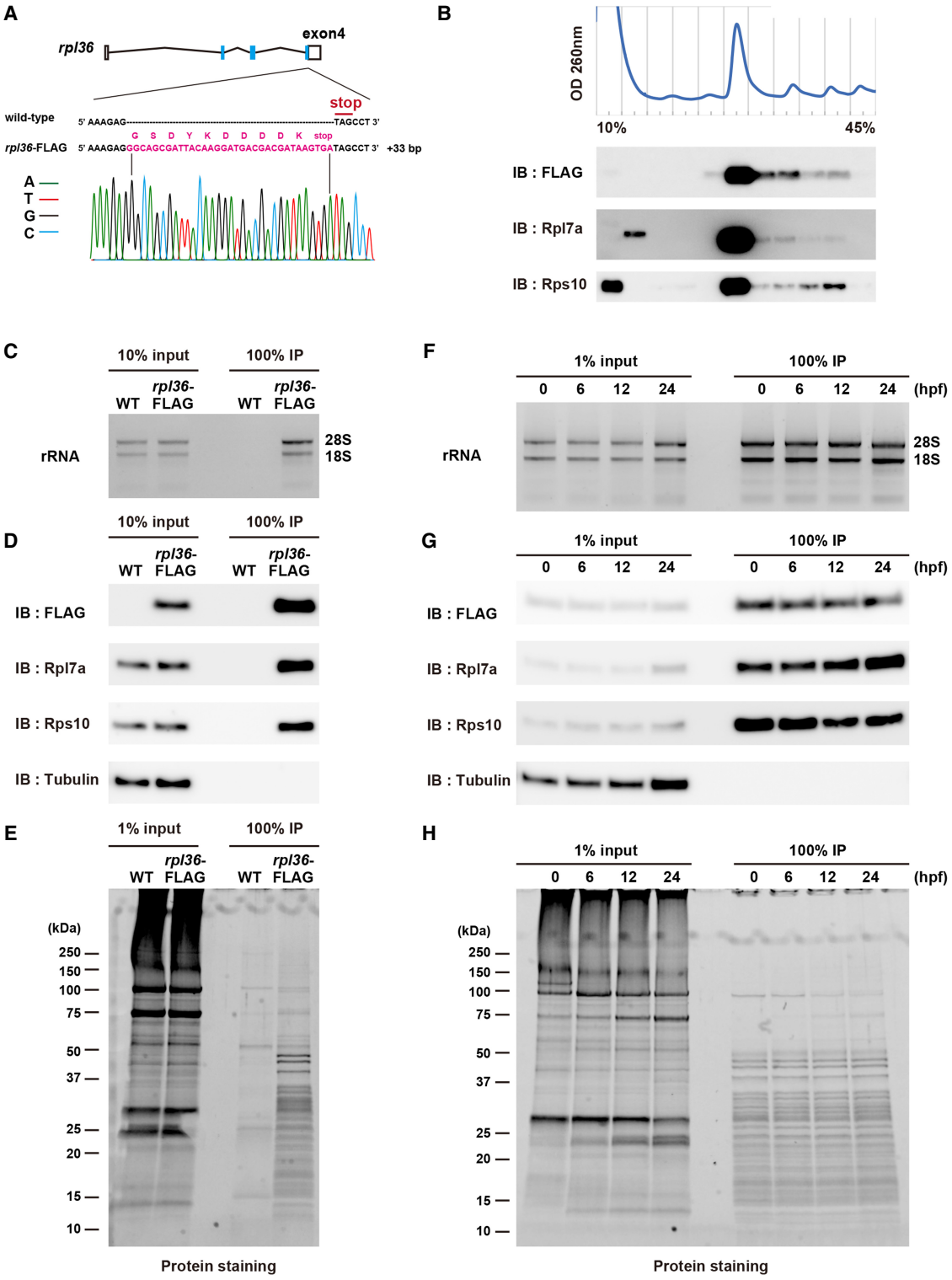

FIGURE 1. Establishment of a ribosome affinity purification system in zebrafish. (*A*) Scheme of a FLAG-tagged *rpl36* gene locus. Genome sequences around the stop codon of wild-type (WT) and *rpl36*-FLAG strains are shown. The sequence chromatogram of *rpl36*-FLAG embryos is indicated *below*. (*B*) Representative polysome profiles of *rpl36*-FLAG embryos at 24 hpf. The distribution patterns of ribosomal proteins are indicated *below*. (*C–E*) Validation of the ribosome purification system with WT and *rpl36*-FLAG embryos at 24 hpf. Total lysates (input) and FLAG-immunoprecipitants (IPs) were subjected to RNA electrophoresis (*C*), immunoblotting analysis using antibodies against the indicated proteins (*D*), and protein staining (*E*). (*F–H*) Validation of the ribosome purification system during various developmental stages. The developmental time points are indicated *above* as hpf. Total lysates (input) and FLAG-IPs were subjected to RNA electrophoresis (*F*), immunoblotting analysis using antibodies against the indicated proteins (*G*), and protein staining (*H*).

of *rpl36*-FLAG embryonic lysate showed that Rpl36-FLAG was incorporated in the functioning 60S subunit: Rpl36-FLAG was detected in 60S, 80S monosome, and polysome fractions (Fig. 1B). After that, we carried out FLAG-immunoprecipitation using 24-h post-fertilization (hpf) embryos, and we verified the purification of ribosomes using three methods. First, electrophoresis of the immunoprecipitated RNA revealed that both 18S and 28S rRNAs were purified from *rpl36*-FLAG embryos (Fig. 1C). Second, immunoblotting analysis showed that a large ribosomal subunit protein Rpl7a/eL8 and a small ribosomal subunit protein Rps10/eS10 were copurified with Rpl36-FLAG (Fig. 1D). Third, protein staining showed that proteins that were <50 kDa, which is the size of the most of ribosomal proteins (Martini and Gould 1975), were copurified with Rpl36-FLAG (Fig. 1E). Hence, the established *rpl36*-FLAG strain enabled us to purify ribosomes from zebrafish embryos by FLAG-immunoprecipitation.

We carried out FLAG-immunoprecipitation using the same number of embryos at 0, 6, 12, and 24 hpf to verify if our ribosome purification system is applicable to samples from various developmental stages. Ribosomal components were detected in the FLAG-immunoprecipitants at comparable levels throughout all developmental stages (Fig. 1F–H). Mass spectrometry analysis of the FLAG-IPs detected the most ribosomal proteins of small and large subunits in all developmental stages investigated (Supplemental Fig. S2A). This analysis also detected various nonribosomal proteins involved in translation, such as Pabpc1a, Ddx6, and eEF1a (Supplemental Fig. S2B; Supplemental Table S1). Immunoblotting analysis further confirmed the copurification of these proteins with the FLAG-immunoprecipitated ribosomes (Supplemental Fig. S2C). These findings suggest that we can purify the ribosome complex engaging in translation from zebrafish embryos at various developmental stages by FLAG-immunoprecipitation using the *rpl36*-FLAG strain.

Detection of ribosome ubiquitination under normal and stress conditions

After developing a ribosome purification system in zebrafish embryos, we considered this system to analyze the ubiquitination status of the ribosome. We performed immunoblotting analysis using an anti-Ubiquitin antibody on FLAG-IPs obtained from 24 hpf WT and *rpl36*-FLAG embryos. Several ubiquitination signals were detected in the FLAG-IP from *rpl36*-FLAG embryos (Fig. 2A). As mentioned above, the FLAG-IP contains not only ribosomes but also ribosome- or mRNA-associated proteins. Therefore, we performed FLAG-immunoprecipitation using the high-salt wash buffer to minimize the copurification of ribosome- and mRNA-associated factors (Supplemental Fig. S3A). When FLAG-IP was washed vigorously, we found that Ddx6 and eEF1a were not copurified, but the ubiquitination

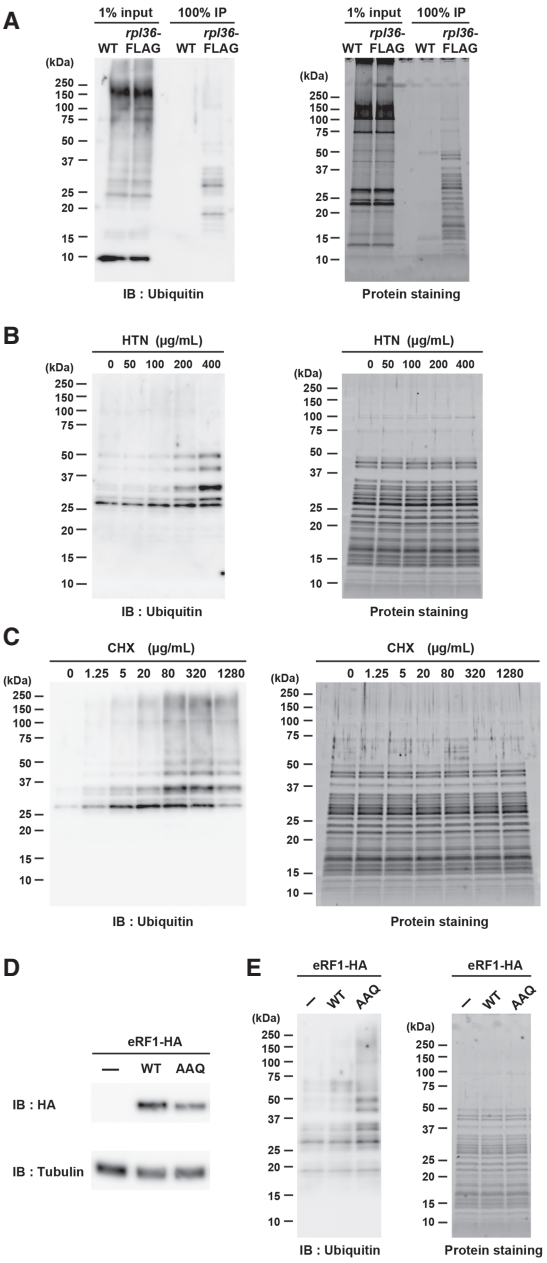

FIGURE 2. Detection of ribosome ubiquitination under normal and stress conditions. (*A*) Detection of ribosome ubiquitination. Total lysates (input) and FLAG-IPs obtained from WT and *rpl36*-FLAG embryos at 24 hpf were subjected to immunoblotting analysis with an anti-Ubiquitin antibody (*left*) and protein staining (*right*). (*B*) Analysis of ribosome ubiquitination under harringtonine (HTN) treatment. FLAG-IPs were subjected to immunoblotting analysis with an anti-Ubiquitin antibody (*left*) and protein staining (*right*). HTN concentrations are indicated *above*. (*C*) Analysis of ribosome ubiquitination under cycloheximide (CHX) treatment. FLAG-IPs were subjected to immunoblotting analysis with an anti-Ubiquitin antibody (*left*) and protein staining (*right*). CHX concentrations are indicated *above*. (*D*,*E*) Analysis of ribosome ubiquitination in the presence of mutant release factor eRF1-AAQ. Total lysates were subjected to immunoblotting analysis of eRF1-HA and Tubulin (*D*). FLAG-IPs were subjected to immunoblotting analysis with an anti-Ubiquitin antibody (*E*, *left*) and protein staining (*E*, *right*).

signals remained the same (Supplemental Fig. S3A,B). Despite the possibility that some ubiquitination signals originate from elements that are closely associated with the ribosome, as shown by Pabpc1 (Supplemental Fig. S3A), we assumed that the majority of signals were caused by the ubiquitination of core ribosomal proteins.

Ribosomes are subjected to ubiquitination upon translational stresses (Higgins et al. 2015; Simms et al. 2017; Juszkiewicz et al. 2018; Garshott et al. 2021; Garzia et al. 2021; Oltion et al. 2023). We thus investigated whether our ribosome purification system can detect ribosome ubiquitination triggered by translation inhibitors, which are known to enhance ribosome ubiquitination. HTN causes Rps2/uS5 and Rps3/uS3 ubiquitination, presumably due to ribosome stalling on the initiation codon (Garshott et al. 2021; Garzia et al. 2021). Following these reports, we treated *rpl36*-FLAG embryos with different concentrations of HTN and analyzed FLAG-IPs with an anti-Ubiquitin antibody. A significant dose-dependent increase in ubiquitination signals was caused by HTN treatment (Fig. 2B). We assumed that HTN caused ribosome stalling on the initiation codon, thereby inducing ribosome ubiquitination, as observed in mammalian cells. We next treated *rpl36*-FLAG embryos with a translation elongation inhibitor CHX. Treatment of elongation inhibitors with intermediate concentrations causes ribosome collisions and induces Rps10/eS10 and Rps3/uS3 ubiquitination (Simms et al. 2017; Juszkiewicz et al. 2018). In fact, we observed that ubiquitination signals were up-regulated as CHX concentration increased, reaching the maximum intensity at 80–320 µg/mL (Fig. 2C). The signals decreased at the highest concentration (1280 µg/mL), probably because the majority of ribosomes stalled at this concentration and fewer collisions were induced, as observed in other organisms (Juszkiewicz et al. 2018).

As an alternative approach, we took advantage of a GGQ motif mutant of a eukaryotic release factor (eRF1-AAQ) that stalls the ribosome on termination codons and induces Rps10/eS10 ubiquitination (Juszkiewicz et al. 2018). Fertilized eggs from the *rpl36*-FLAG strain were injected with mRNAs encoding carboxy-terminally Hemagglutinin (HA)-tagged WT Etf1b (a zebrafish ortholog of eRF1) or Etf1b-AAQ mutant (Fig. 2D). As expected, ubiquitination signals increased at 6 hpf when eRF1-AAQ was injected (Fig. 2E). These results indicate that, like other organisms, zebrafish embryos exhibit fluctuations in ribosome ubiquitination levels in response to translational stresses. Our FLAG-immunoprecipitation system is thus suitable for monitoring the dynamics of ribosome ubiquitination occurring in zebrafish embryos.

Ribosome ubiquitination level changes during zebrafish development

Next, we purified ribosomes from embryonic (0 hpf to 2-d post-fertilization [dpf]) and larval stages (3–7 dpf) and analyzed the dynamics of ribosome ubiquitination during zebrafish development. Ribosome ubiquitination signals temporally changed during development (Fig. 3A,B). Although it was most noticeable in the signal above 25 kDa (Fig. 3A, arrowhead), this tendency was present in all the signals detected between 25 and 50 kDa (Fig. 3A, bracket). Immediately following spawning (0 hpf), the level of ribosome ubiquitination was low; but as development proceeded, it gradually increased. The ubiquitination level reached the maximum intensity at 24 hpf and then decreased toward 7 dpf (Fig. 3B). These findings indicate that during development, the level of ribosome ubiquitination fluctuates.

To understand the characteristics of the ubiquitination signals, we investigated which subunit of the ribosome was linked with the detected ubiquitination signals. We performed FLAG-immunoprecipitation using the EDTA-containing buffer to dissociate 80S ribosomes into 40S and 60S subunits. Because the FLAG-tag was attached to the 60S ribosomal protein Rpl36/eL36, only 60S subunit components were purified in the presence of EDTA (Fig. 3C). The amount of the purified 60S subunit reduced to approximately 25%–50% compared to the yield in the absence of EDTA, suggesting that the ribosomes purified in the absence of EDTA contained 80S ribosomes forming polysomes. We therefore compared the ubiquitination signals linked with the purified 60S (+EDTA) to that of serial dilutions of 80S (−EDTA) and found that most of the signals disappeared in the purified 60S (Fig. 3D). Only the signal around 50 kDa remained in the +EDTA condition, indicating that this signal was derived from the 60S subunit (Fig. 3D, arrowhead). EDTA per se did not reduce ubiquitination signals artificially because the signals were retained when the FLAG-IP was prepared in the EDTA-free condition and then incubated with EDTA (Supplemental Fig. S3C). Hence, most ubiquitination signals were associated with the 80S ribosome in a 40S subunit-dependent manner. These findings suggest that during zebrafish development, the 40S ribosomal subunit components are differently ubiquitinated.

Znf598 promotes ribosome ubiquitination during development

Several E3 ubiquitin ligases ubiquitinate ribosomal proteins in the 40S subunit (Panasenko and Collart 2012; Garzia et al. 2017, 2021; Juszkiewicz et al. 2018; Sugiyama et al. 2019; Li et al. 2022; Oltion et al. 2023). Unfortunately, our initial mass spectrometry analysis detected no E3 ubiquitin ligases known to ubiquitinate ribosomal proteins (Supplemental Table S1). Since we had already generated a *znf598* mutant zebrafish strain (Mishima et al. 2022), we utilized this strain to investigate whether Znf598 affects the ribosome ubiquitination during zebrafish development. We crossed the *rpl36*-FLAG strain with the *znf598* mutant strain and

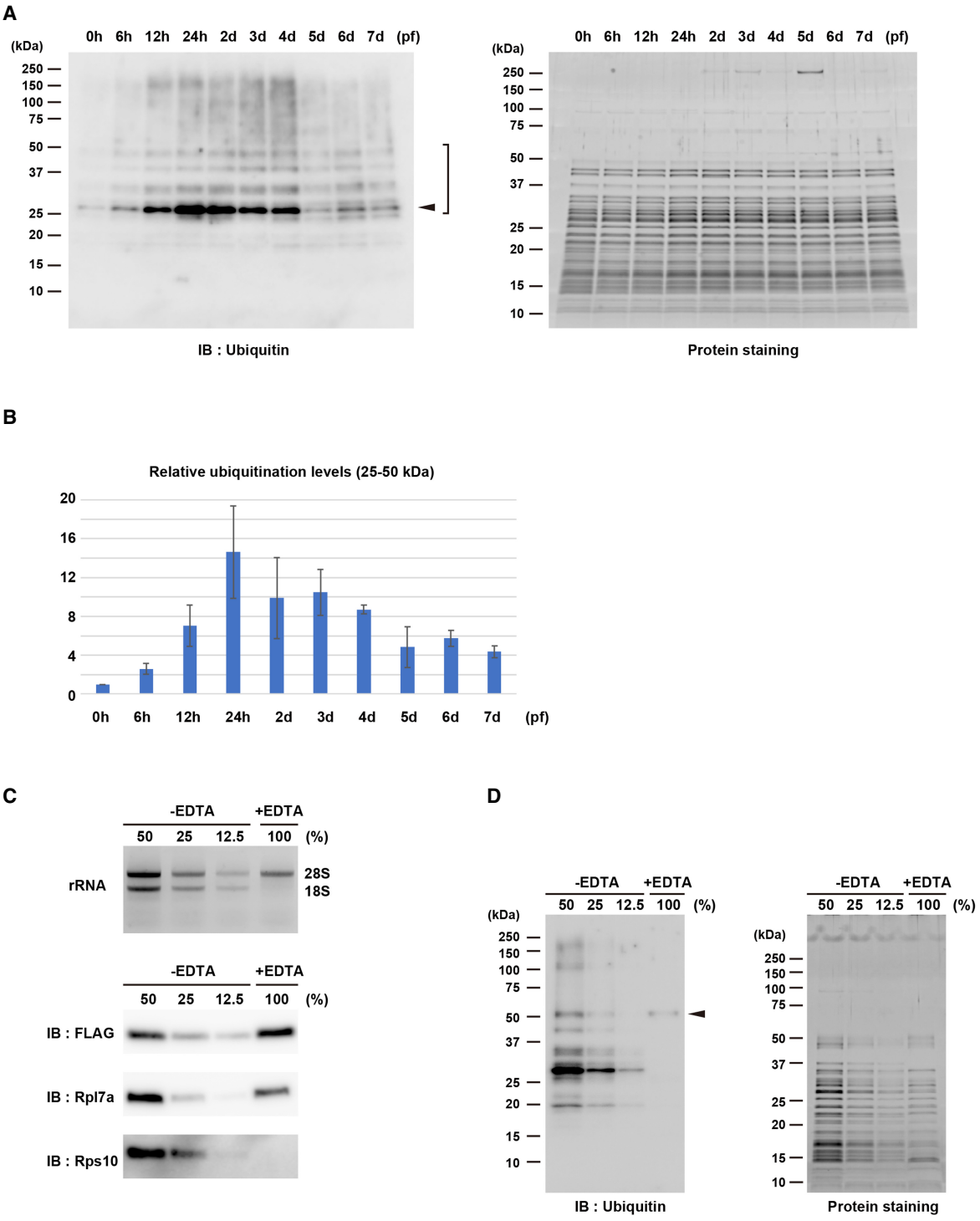

FIGURE 3. Ribosome ubiquitination level changes during zebrafish development. (*A*) Detection of ribosome ubiquitination during development. FLAG-IPs from various developmental stages were subjected to immunoblotting analysis with an anti-Ubiquitin antibody (*left*) and protein staining (*right*). Arrowhead indicates the most noticeable ubiquitination signal. Ubiquitination signals between 25 and 50 kDa were reproducibly detected (bracket). The developmental time points are indicated *above* as hpf or dpf. (*B*) A bar graph shows ubiquitination levels relative to 0 hpf. Ubiquitination signals between 25 and 50 kDa in (*A*, *left*) were normalized by corresponding protein amounts in (*A*, *right*). The average of three independent experiments is indicated. The error bars indicate the standard deviation. (*C*) Validation of 60S subunits purification. FLAG-IPs in the presence (+) or absence (–) of EDTA were subjected to RNA electrophoresis (*upper*) and immunoblotting analysis of ribosomal proteins (*lower*). The –EDTA samples were serially diluted as indicated *above*. (*D*) Detection of ribosome ubiquitination in the presence (+) or absence (–) of EDTA. FLAG-IPs in (*C*) were subjected to immunoblotting analysis with an anti-Ubiquitin antibody (*left*) and protein staining (*right*). Arrowhead indicates a ubiquitination signal derived from 60S subunits.

obtained fish carrying a heterozygous *rpl36*-FLAG allele and a homozygous *znf598* mutant allele. Crossing female and male of this genotype, we obtained maternal-zygotic *znf598* (MZ*znf598*) mutant embryos expressing Rpl36-FLAG (hereafter called MZ*znf598*;*rpl36*-FLAG embryos). The ubiquitination status of ribosomes purified from MZ*znf*598;*rpl36*-FLAG embryos and *rpl36*-FLAG embryos at 0 and 24 hpf was examined. Although the initial ubiquitination levels at 0 hpf were comparable, the increase of the ubiquitination level at 24 hpf was attenuated in MZ*znf598*;*rpl36*-FLAG embryos (Fig. 4A,B). On the other hand, we investigated whether overexpressing Znf598 increased the ubiquitination level of ribosomes. The ubiquitination level was increased by overexpression of WT Znf598 but not by RING domain-mutated Znf598 (cysteines 13 and 16 were substituted with alanines; C13/16A) (Fig. 4C,D). These results indicate that Znf598 enhances ribosome ubiquitination during zebrafish development.

Znf598 promotes Rps10/eS10 ubiquitination in zebrafish embryos

Next, we tried identifying ribosomal protein(s) that were ubiquitinated by Znf598 during zebrafish development. Due to the low ubiquitination levels of ribosomal proteins, our initial mass spectrometry analysis with FLAG-IPs obtained from 0 to 24 hpf embryos was unable to reliably identify ubiquitinated ribosomal proteins (data not shown). Therefore, we overexpressed Znf598 to maximize the ubiquitination level at 24 hpf and subjected the FLAG-IPs to mass spectrometry analysis. We found that the intensity of an Rps10/eS10 peptide with a di-glycine remnant at lysine 139 was increased in two independent Znf598 overexpression samples (Fig. 4E,F). To examine whether Rps10/eS10 was indeed ubiquitinated at 24 hpf in a Znf598-dependent manner, we purified ribosomes and detected Rps10/eS10 by immunoblotting analysis in three conditions: *rpl36*-FLAG, *rpl36*-FLAG with Znf598 overexpression, and MZ*znf598*;*rpl36*-FLAG (Fig. 4G,H). The major signal that appeared below 20 kDa (Fig. 4H, left) was consistent with the predicted molecular weight of zebrafish Rps10/eS10 (18.9 kDa). Additionally, in *rpl36*-FLAG embryos, a minor signal above 25 kDa was detected, which we ascribed to monoubiquitinated Rps10/eS10. Overexpression of Znf598 increased this minor signal and induced an additional slower migrating signal attributable to Rps10/eS10 attached with two ubiquitin molecules. In contrast, these additional signals were not detected in MZ*znf598*;*rpl36*-FLAG embryos. The same result was observed with exogenously expressed Rps10/eS10 with an HA-tag at the carboxyl terminus (Supplemental Fig. S4A,B). These results indicate that Rps10/eS10 is ubiquitinated at 24 hpf in a Znf598-dependent manner.

While our mass spectrometry analysis detected lysine 139 in Rps10/eS10 as a potential ubiquitination site by Znf598 in zebrafish, lysines 138 and 139 (corresponding to lysines 139 and 140 in zebrafish) are ubiquitinated in a ZNF598-dependent manner in mammals (Garzia et al. 2017; Sundaramoorthy et al. 2017). To validate ubiquitination site(s) in zebrafish Rps10/eS10 further, we substituted lysine 139 and/or 140 with arginine in Rps10-HA and overexpressed them in *rpl36*-FLAG embryos. We found that the ubiquitinated signal of Rps10-HA was not detectable in K139R single and K139/140R double mutants (Supplemental Fig. S4C). In contrast, the K140R single mutant reduced the ubiquitinated signal only marginally. We conclude that lysine 139 in Rps10/eS10 is a major ubiquitination site by Znf598 in zebrafish embryos, although we do not rule out the possibility that lysine 140 serves as an additional ubiquitination site.

During zebrafish development, Rps10/eS10 ubiquitination is crucial for establishing the ribosome ubiquitination pattern

To characterize the contribution of Rps10/eS10 ubiquitination to the overall ribosome ubiquitination pattern during development, we substituted lysine 139 and 140 codons of the endogenous *rps10* locus with arginine codons by CRISPR–Cas9-mediated genome editing (*rps10* K139/140R) (Fig. 5A). Homozygous *rps10* K139/140R fish reached adulthood, and we obtained a homozygous *rps10* K139/140R strain with a heterozygous *rpl36*-FLAG allele. Consistent with the experiments using Rps10-HA (Supplemental Fig. S4C), the ubiquitinated signals of endogenous Rps10/eS10 were not detected in ribosomes purified from the *rps10* K139/140R;*rpl36*-FLAG embryos, even with Znf598 overexpression (Fig. 5B,C). We then compared the overall ubiquitination pattern of purified ribosomes at 24 hpf. Similar to the ribosomes purified from MZ*znf598*;*rpl36*-FLAG embryos, multiple ubiquitination signals were reduced in ribosomes purified from *rps10* K139/140R;*rpl36*-FLAG embryos compared to ribosomes containing WT Rps10/eS10 (Fig. 5D). Considering the molecular weight of the ubiquitinated Rps10/eS10 forms detected in the Rps10/eS10 immunoblotting analysis (Fig. 5C), two ubiquitination signals were attributable to ubiquitinated forms of Rps10/eS10 (Fig. 5D, black arrowheads). Indeed, the signal that probably derived from the Rps10/eS10 with two ubiquitin molecules was not detected in *rps10* K139/140R;*rpl36*-FLAG and MZ*znf598*;*rpl36*-FLAG embryos. The signal that probably derived from the monoubiquitinated Rps10/eS10 was reduced but still present in both *rps10* K139/140R;*rpl36*-FLAG and MZ*znf598*;*rpl36*-FLAG embryos, likely due to an overlap with other ubiquitinated protein(s). Notably, intensities of three additional signals were also reduced in *rps10* K139/140R;*rpl36*-FLAG and MZ*znf598*;*rpl36*-FLAG embryos (Fig. 5D, white arrowheads). It is plausible that there are additional ribosomal proteins whose ubiquitination depends on Znf598-

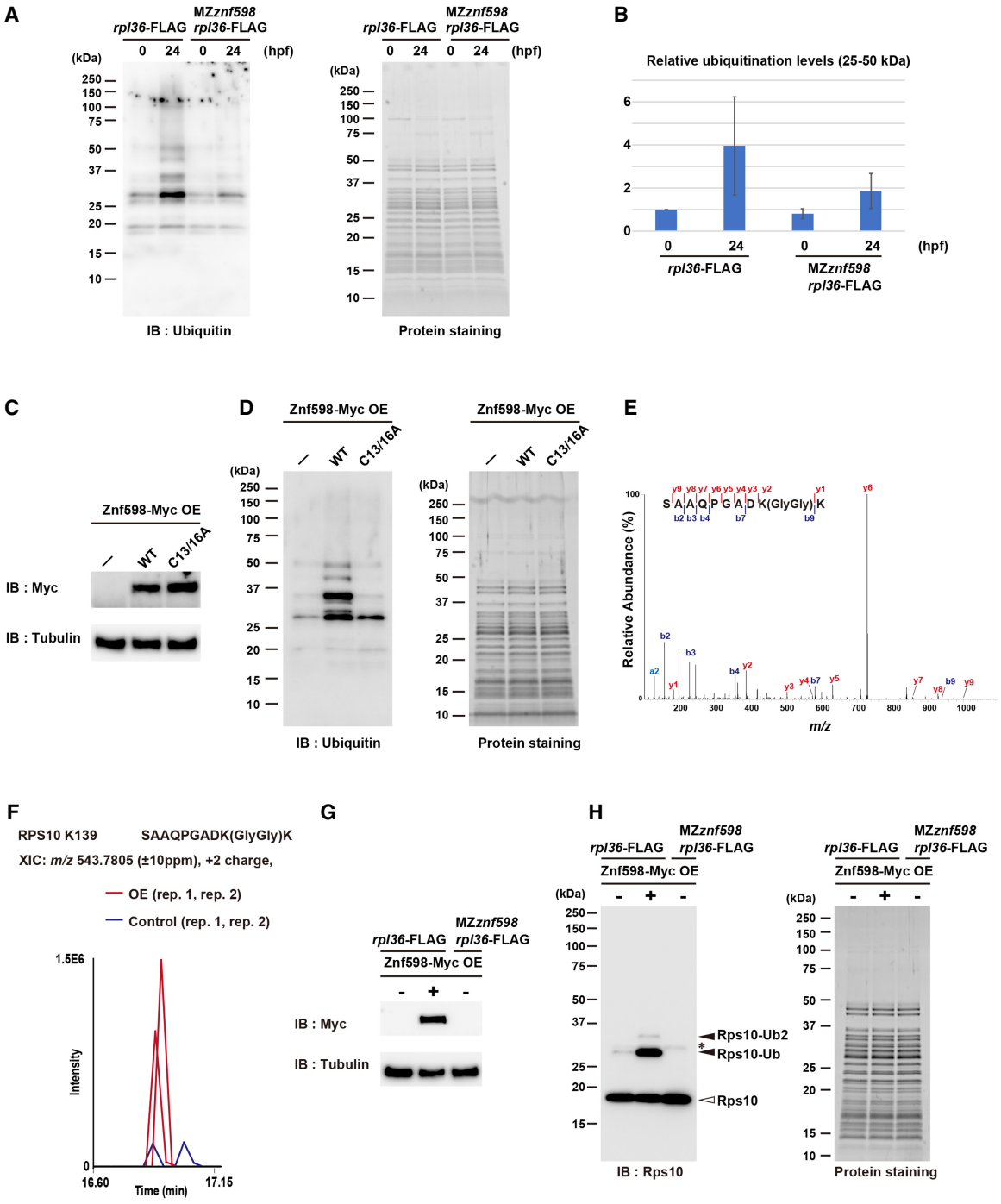

FIGURE 4. Znf598 promotes ribosome ubiquitination during development. (*A*) Comparison of ribosome ubiquitination levels of *rpl36*-FLAG and MZ*znf598*;*rpl36*-FLAG embryos. FLAG-IPs from 0 and 24 hpf embryos were subjected to immunoblotting analysis with an anti-Ubiquitin antibody (*left*) and protein staining (*right*). The developmental time points are indicated *above* as hpf. (*B*) A bar graph shows ubiquitination levels relative to that of *rpl36*-FLAG embryos at 0 hpf. Ubiquitination signals between 25 and 50 kDa in (*A*, *left*) were normalized by corresponding protein amounts in (*A*, *right*). The average of three independent experiments is indicated. The error bars indicate the standard deviation. (*C*,*D*) Comparison of ribosome ubiquitination levels with or without Znf598 overexpression. Total lysates were subjected to immunoblotting analysis of Znf598-Myc and Tubulin (*C*). FLAG-IPs were subjected to immunoblotting analysis with an anti-Ubiquitin antibody (*D*, *left*) and protein staining (*D*, *right*). (*E*) A representative MS/MS spectrum of Rps10/eS10 di-glycyl K139. (*F*) MS-based quantification of a ubiquitinated peptide of Rps10/eS10 containing di-glycyl K139 under Znf598 OE (red) and control (blue) conditions. (*G*,*H*) Detection of Rps10/eS10 ubiquitination. Total lysates were subjected to immunoblotting analysis of Znf598-Myc and Tubulin (*G*). FLAG-IPs were subjected to immunoblotting analysis with an anti-Rps10 antibody (*H*, *left*) and protein staining (*H*, *right*). White and black arrowheads indicate nonubiquitinated or ubiquitinated Rps10/eS10 signals, respectively. The asterisk indicates a nonspecific signal.

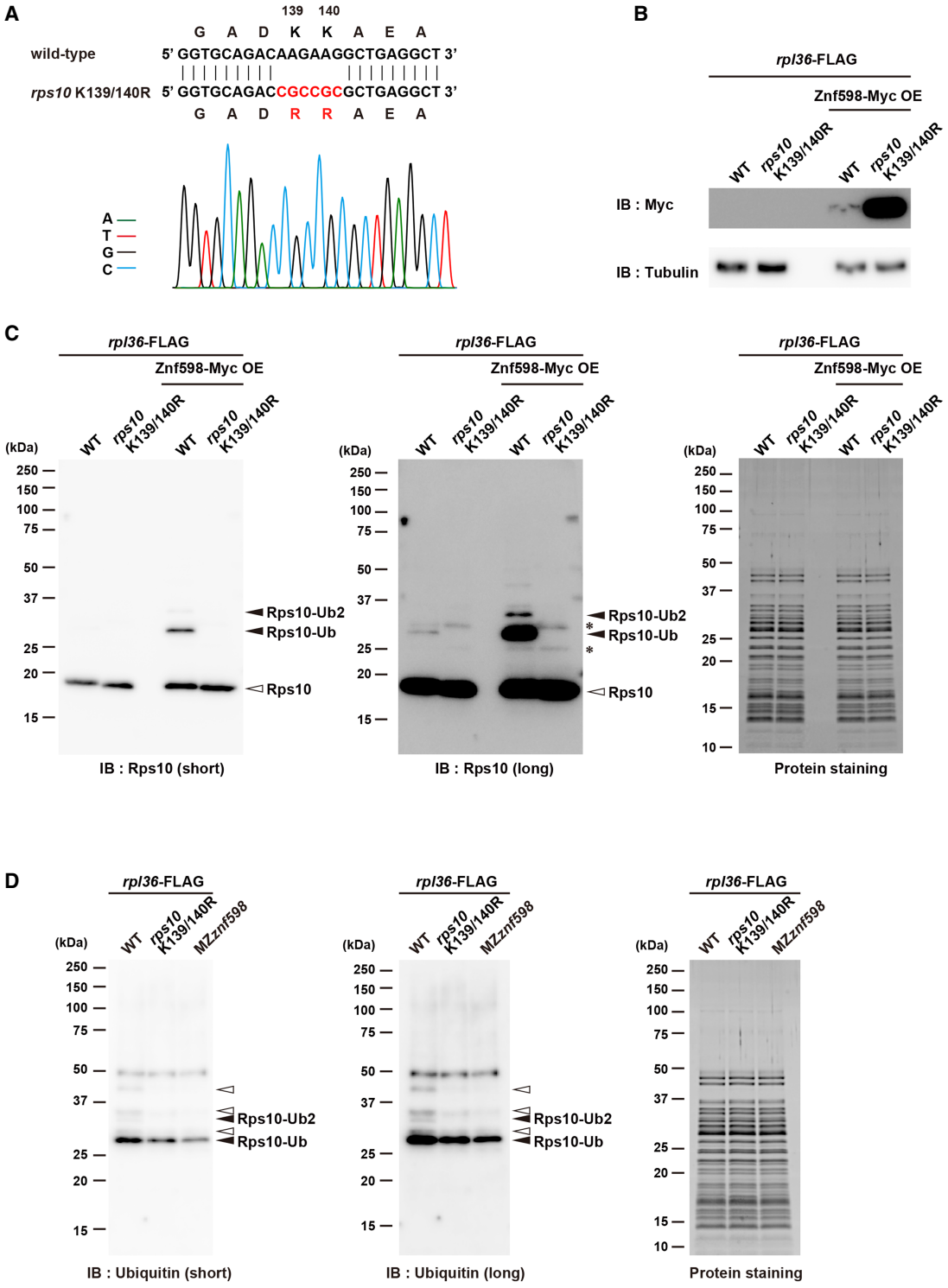

FIGURE 5. During zebrafish development, Rps10/eS10 ubiquitination is crucial for establishing the ribosome ubiquitination pattern. (*A*) Alignment of WT and K139/140R *rps10* sequences. The sequencing chromatogram of the *rps10* K139/140R embryos is indicated *below*. (*B*, *C*) Detection of Rps10/eS10 ubiquitination with or without Znf598 overexpression in *rpl36*-FLAG and *rps10* K139/140R;*rpl36*-FLAG embryos. Total lysates were subjected to immunoblotting analysis of Znf598-Myc and Tubulin (*B*). FLAG-IPs were subjected to immunoblotting analysis with an anti-Rps10 antibody (*C*, *left* and *middle*) and protein staining (*C*, *right*). White and black arrowheads indicate nonubiquitinated or ubiquitinated Rps10/eS10 signals, respectively. Asterisks indicate nonspecific signals. (*D*) Comparison of ribosome ubiquitination pattern in *rpl36*-FLAG, *rps10* K139/140R;*rpl36*-FLAG, and MZ*znf598*;*rpl36*-FLAG embryos. FLAG-IPs were subjected to immunoblotting analysis with an anti-Ubiquitin antibody (*left* and *middle*) and protein staining (*right*). Black arrowheads indicate putative ubiquitinated Rps10/eS10 signals. White arrowheads indicate reduced ubiquitination signals in *rps10* K139/140R;*rpl36*-FLAG and MZ*znf598*;*rpl36*-FLAG embryos.

mediated Rps10/eS10 ubiquitination. In mammalian cells, ubiquitination levels of Rps20/uS10 and Rps3/uS3 are reduced in the absence of Rps10/eS10 ubiquitination (Garshott et al. 2020; Meyer et al. 2020). Similarly, the ubiquitination of Rps3/uS3 is necessary for the ubiquitination of Rps2/uS5 (Meyer et al. 2020). To investigate the ubiquitination levels of these ribosomal proteins, HA-tagged Rps20/uS10, Rps3/uS3, and Rps2/uS5 were overexpressed in *rpl36*-FLAG and *rps10* K139/140R;*rpl36*-FLAG embryos. These ribosomal proteins were ubiquitinated in *rpl36*-FLAG embryos at 24 hpf, while their ubiquitinated signals were barely detectable in *rps10* K139/140R;*rpl36*-FLAG embryos (Supplemental Fig. S5A–C). Although we were unable to identify each ubiquitination site detected by an anti-Ubiquitin antibody (Fig. 5D), Rps20/uS10, Rps3/uS3, and Rps2/uS5 ubiquitination was likely dependent on Rps10/eS10 ubiquitination.

To further test the requirement of Znf598-mediated Rps10/eS10 ubiquitination for establishing the entire ubiquitination pattern of the ribosome, we performed two experiments. First, we compared ubiquitination signals in *rpl36*-FLAG and *rps10* K139/140R;*rpl36*-FLAG embryos under the Znf598-overexpressed condition (Supplemental Fig. S6A). Whereas multiple ubiquitination signals were enhanced by overexpression of Znf598 in *rpl36*-FLAG embryos, the increase of these signals was significantly suppressed in *rps10* K139/140R;*rpl36*-FLAG embryos. Second, we investigated the ubiquitination levels under translationally stressed conditions in *rpl36*-FLAG, *rps10* K139/140R;*rpl36*-FLAG and MZ*znf598*;*rpl36*-FLAG embryos (Supplemental Fig. S6B–E). The enhancement of ribosome ubiquitination levels by CHX treatment and overexpression of eRF1-AAQ was attenuated in both *rps10* K139/140R;*rpl36*-FLAG and MZ*znf598*;*rpl36*-FLAG embryos, albeit to different extents (Supplemental Fig. S6C,E). In contrast, HTN treatment increased ribosome ubiquitination levels in *rps10* K139/140R;*rpl36*-FLAG and MZ*znf598*;*rpl36*-FLAG embryos comparable to *rpl36*-FLAG embryos (Supplemental Fig. S6B). These results further support our assumption that Rps10/eS10 ubiquitination is a prerequisite for multiple ubiquitination events promoted by Znf598.

Given the critical role of Rps10/eS10 ubiquitination by Znf598 for establishing the ribosome ubiquitination pattern at 24 hpf, we wondered if Rps10/eS10 ubiquitination per se fluctuates during development. To test this possibility, we performed immunoblotting analysis to examine Rps10/eS10 ubiquitination from 0 to 24 hpf. At 0 hpf, the monoubiquitinated Rps10/eS10 signal was barely detectable; however, it gradually increased until 24 hpf in *rpl36*-FLAG embryos, mirroring the increase in the whole ribosome ubiquitination levels (Figs. 3A and 6A). These Rps10/eS10 monoubiquitinated signals were completely abolished in *rps10* K139/140R;*rpl36*-FLAG embryos. Next, we analyzed Rps10/eS10 ubiquitination in larval stages. The Rps10/eS10 monoubiquitination levels peaked between 1 and 3 dpf and gradually decreased toward 7 dpf (Fig. 6B), similar to the whole ribosome ubiquitination levels (Fig. 3A). Overall, these results demonstrate that Rps10/eS10 ubiquitination by Znf598 occurs dynamically after fertilization and contributes directly and indirectly to establishing the overall ribosome ubiquitination pattern during zebrafish development.

DISCUSSION

In this study, we established a novel ribosome affinity purification system in zebrafish by introducing a FLAG-tag into endogenous Rpl36/eL36. Using this system, we affinity purified almost fully assembled 80S ribosomes from zebrafish embryos at different developmental stages. In comparison to the standard ribosome purification methods using sucrose gradient ultracentrifugation, this method offers certain advantages due to the simplicity of the experimental process, good repeatability, and efficiency (20% of the input).

Transgenic zebrafish strains expressing an exogenous copy of EGFP-fused Rpl10a/uL1 were generated previously and were utilized for purifying ribosome-associated mRNAs (Tryon et al. 2013). However, engineering an endogenous ribosomal gene locus with an affinity tag insertion has been challenging in zebrafish. Our *rpl36*-FLAG strain is the first example of tagging an endogenous ribosomal protein in zebrafish, enabling the purification of ribosomes with minimum perturbation of the stoichiometry of ribosomal proteins. Rpl36-FLAG was incorporated into the 60S subunit efficiently and allowed the purification of 80S ribosomes to analyze ubiquitination status. Our *rpl36*-FLAG strain will assist in the analysis of ribosome modifications as well as ribosome components, ribosome-associated proteins, and ribosome-associated mRNAs during zebrafish development, even though it is uncertain whether the ribosome containing Rpl36-FLAG is functionally identical to the WT ribosome.

Combining the ribosome affinity purification approach with genetic mutants, we revealed the complex and dynamic nature of ribosome ubiquitination during zebrafish development. The ubiquitination level of ribosomes was at its lowest just after spawning, indicating that ribosomes in eggs are mostly stored without ubiquitination. Before fertilization, global translation is silenced, and ribosomes are kept in a dormant state (Leesch et al. 2023). The cotranslational ubiquitination pathways should not be at work in such a situation. Hence, the low level of ribosome ubiquitination in eggs may reflect the absence of cotranslational ribosome ubiquitination during oogenesis. Alternatively, but not exclusively, the activity of ribosome deubiquitinating enzymes such as USP10, OTUD1, USP21, and OTUD3 (Garshott et al. 2020; Meyer et al. 2020; Snaurova et al. 2022) may predominate over ribosome ubiquitination activity during oogenesis, keeping the ribosome less ubiquitinated. In any case, our data indicate that the maternal ribosome starts from a naïve ubiquitination state in zebrafish embryogenesis.

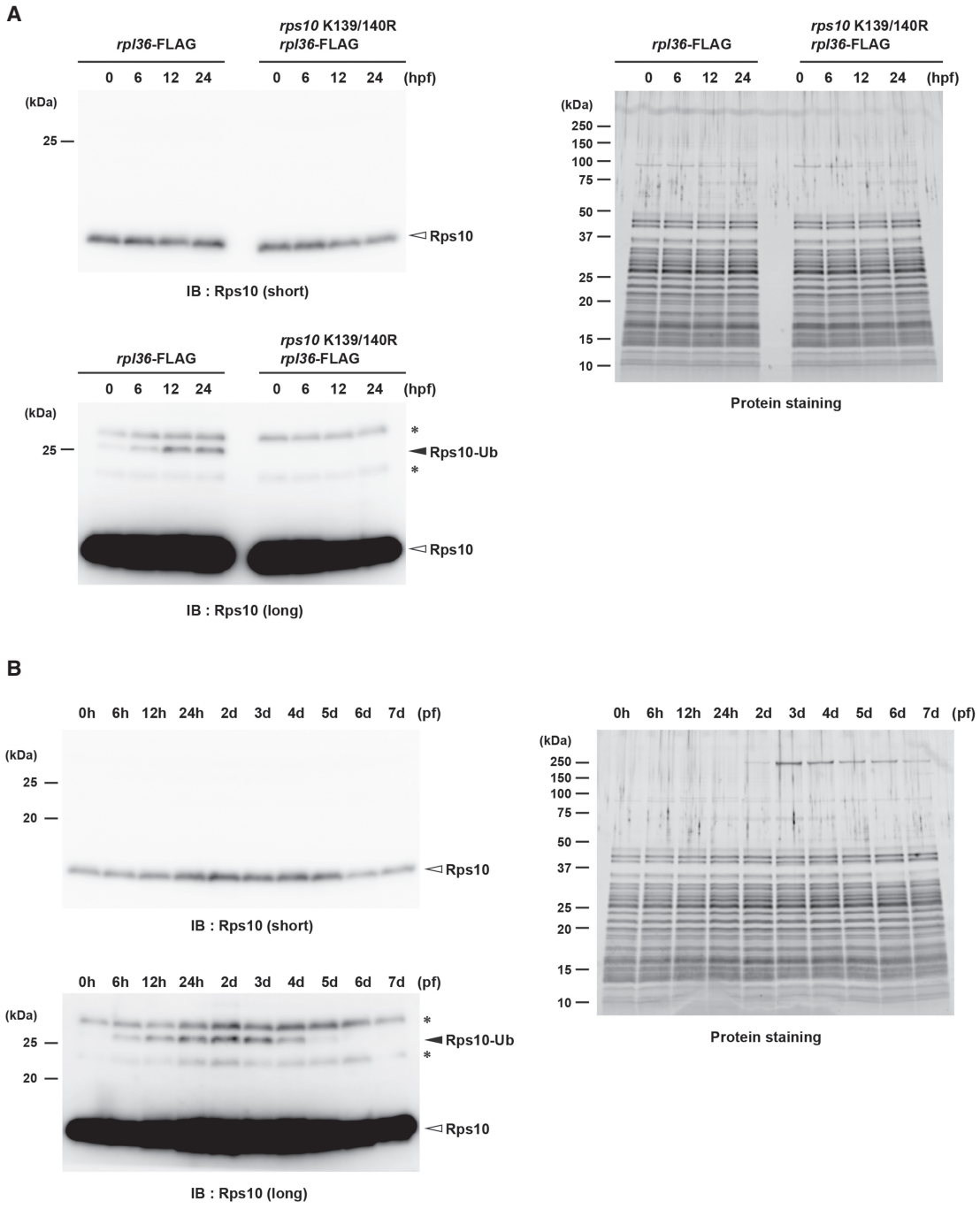

FIGURE 6. Rps10/eS10 ubiquitination level temporally changes during development. (*A*) Detection of Rps10/eS10 ubiquitination from 0 to 24 hpf embryos. FLAG-IPs were subjected to immunoblotting analysis with an anti-Rps10 antibody (*left*) and protein staining (*right*). The developmental time points are indicated *above* as hpf. White and black arrowheads indicate nonubiquitinated or ubiquitinated Rps10/eS10 signals, respectively. Asterisks indicate nonspecific signals. (*B*) Detection of Rps10/eS10 ubiquitination during development. FLAG-IPs were subjected to immunoblotting analysis with an anti-Rps10 antibody (*left*) and protein staining (*right*). The developmental time points are indicated *above* as hpf or dpf. White and black arrowheads indicate nonubiquitinated or ubiquitinated Rps10/eS10 signals, respectively. Asterisks indicate nonspecific signals.

In the present study, we revealed that multiple ribosome ubiquitination signals gradually increased after fertilization, and ubiquitination of Rps10/eS10 by Znf598 contributed to this process. As ZNF598 plays a pivotal role in RQC and its ubiquitination sites in Rps10/eS10 are highly conserved (Garzia et al. 2017; Juszkiewicz and Hegde 2017; Sundaramoorthy et al. 2017), it is likely that the ribosome ubiquitination increases after fertilization in response to ribosome collisions. It is possible that following fertilization, translation activation induces ribosome collisions on stall-

prone mRNAs, and that as collided ribosomes accumulate, Znf598-dependent ribosome ubiquitination increases. Supporting this scenario, ribosome collision sites were detected in more than 1000 mRNA species at 4 hpf (Han et al. 2020). Alternatively, Znf598 may be developmentally regulated. Compared to the lysate of HEK293, ZNF598 accumulates at significantly lower levels in rabbit reticulocytes (Juszkiewicz et al. 2018), indicating that ZNF598 steady-state levels may vary depending on the cellular situation. Considering that the substoichiometric abundance of ZNF598 (Garzia et al. 2017) and Znf598 overexpression in zebrafish embryos increased ribosome ubiquitination at 24 hpf, the Znf598 protein amount can be a major determinant of ribosome ubiquitination levels in response to ribosome collisions. During oxidative stress, inhibition of a deubiquitinating enzyme promotes ribosome ubiquitination (Silva et al. 2015). Therefore, the degree of deubiquitinating enzyme(s) activation or expression is also a critical factor in promoting ribosome ubiquitination. Future research must determine the frequency of ribosome collision and the balance between the expression and activation of the deubiquitinating enzyme(s) and Znf598 during zebrafish development.

A balance between Znf598-mediated ubiquitination and other molecular pathways that recognize collided ribosomes is another factor that potentially affects the ubiquitination levels of the ribosome. ZAKα is recruited to collided ribosomes and phosphorylates p38 and JNK, leading to cell death (Vind et al. 2020; Wu et al. 2020). Additionally, ZAKα recruits GCN1 to collided ribosomes (Wu et al. 2020), and GCN1 further binds to collided ribosomes to provide a scaffold for eIF2α phosphorylation, therefore attenuating global translation initiation and preventing further ribosome collision (Pochopien et al. 2021; Yan and Zaher 2021). EDF1 is an additional collided ribosome sensor and inhibits translation initiation via the GIGYF2–4EHP complex (Juszkiewicz et al. 2020a). Therefore, competition among Znf598, ZAKα, GCN1, and EDF1 on the collided ribosomes may impact the efficiency of ribosome ubiquitination. In addition, several factors are reported to reduce ribosome stalling, such as GTPBP2 and eIF5A (Ishimura et al. 2014; Schuller et al. 2017). We assume that during development, a delicate balance between these multiple factors is not static but rather dynamic and contributes to the changes in the ubiquitination levels of ribosomes.

Although Rps10/eS10 is one of the key ubiquitinated ribosomal proteins in zebrafish embryos, neither loss of Znf598 nor mutations of the ubiquitination sites in Rps10/eS10 abolished ubiquitination signals on the ribosome completely, indicating that Rps10/eS10 alone cannot explain the entire ubiquitination pattern of the ribosome during development. The identity of the remaining ubiquitinated protein(s) needs to be determined. Our data showed that most of the ubiquitination signals were linked with the 40S subunit of the ribosome. Furthermore, the Znf598 mutant and the Rps10 K139/140R mutant not only abolished the Rps10/eS10 ubiquitination per se, but also reduced the additional ubiquitination signals on the ribosome. These findings imply that further ubiquitination events on the 40S subunit require Znf598-mediated Rps10/eS10 ubiquitination as a prerequisite. Indeed, we observed that ubiquitination levels of Rps20/uS10, Rps3/uS3, and Rps2/uS5 decreased in the Rps10 K139/140R mutant. Therefore, as reported in other organisms (Garshott et al. 2020; Meyer et al. 2020), ubiquitination of these ribosomal proteins depends on Znf598-mediated Rps10/eS10 ubiquitination in zebrafish embryos. We speculate that these ubiquitination events may fluctuate during zebrafish development, as observed with Rps10/eS10 ubiquitination. The K139/140R mutation of Rps10/eS10 attenuated multiple ribosome ubiquitination signals under CHX treatment and eRF1-AAQ overexpression, further supporting the presence of hierarchical ubiquitination events. Overall, our data indicate that Znf598-mediated Rps10/eS10 ubiquitination plays a key role in establishing the entire ubiquitination pattern during development.

Ribosome ubiquitination has been studied mainly in cultured cells and yeast under artificially stressed conditions. The present study demonstrated for the first time that Rps10/eS10 is dynamically ubiquitinated in the normal developmental process. One remaining question is the biological relevance of the ribosome ubiquitination dynamics to development. Both the homozygous *znf598* mutant fish and the homozygous *rps10* K139/140R fish had morphologies similar to those of WT fish and had the ability to create offspring on their own. Hence, the requirement of Znf598-mediated Rps10/eS10 ubiquitination during zebrafish development is still unknown. Future research is necessary to identify morphologically undetectable abnormalities in the absence of Znf598-mediated Rps10/eS10 ubiquitination and to determine if the trait develops under translationally stressful conditions.

MATERIALS AND METHODS

Zebrafish husbandry

The zebrafish AB strain was used as a WT strain and maintained according to the animal experiment protocol (2023–37) at Kyoto Sangyo University. Fish were raised and maintained at 28.5°C under standard laboratory conditions with a cycle of 14 h-light and 10 h-dark. The natural breeding method was used to produce fertilized eggs, and embryos were grown in system water at 28.5°C.

Generation of *rpl36*-FLAG and *rps10* K139/140R strains

The zebrafish *rpl36*-FLAG and *rps10* K139/140R strains were generated by CRISPR–Cas9-mediated genome editing. CRISPRscan (Vejnar et al. 2016) was used to predict a single-guide RNA

(sgRNA) targeting exon 4 of the *rpl36* gene locus (ENSDARG00000100588) or exon 5 of the *rps10* gene locus (ENSDARG00000034897). The DNA template for sgRNA synthesis was prepared by PCR using the gene-specific sgRNA primer and the sgRNA tail primer, as shown in Supplemental Table S2. The template was transcribed with T7 RNA Polymerase (Takara) and purified using ProbeQuant G-25 microcolumns (Cytiva). As shown in Supplemental Table S2, the single-stranded oligodeoxynucleotides (ssODNs) were synthesized by Eurofins Genomics. The recombinant Cas9 protein (Takara) and the sgRNA were incubated for 10 min at 37°C and coinjected with the ssODN in one-cell zebrafish embryos (0.45 µg/µL Cas9 protein, 90 ng/µL sgRNA, 0.125 pmol/µL ssODN). Injected embryos were grown into adult fish and crossed with WT fish. Using the appropriate set of primers (Supplemental Table S2), embryos carrying an insertion/substitution in the corresponding gene locus were screened by genotyping PCR, and siblings with potential insertion/substitution were raised. Fin-clipping was used to genotype adult fish, and Sanger sequencing was used to verify that the editing was successful.

Generation of MZ*znf598*;*rpl36*-FLAG and *rps10* K139/140R;*rpl36*-FLAG strains

The *znf598* mutant strain generated previously (Mishima et al. 2022) and the *rps10* K139/140R mutant strain generated in this study were crossed with the *rpl36*-FLAG strain. Heterozygous fish were crossed to generate a homozygous *znf598* mutant or *rps10* K139/140R mutant in the *rpl36*-FLAG heterozygous background.

Plasmid construction

The primer sequences and plasmids used in this study are shown in Supplemental Tables S2 and S3, respectively. The ORFs of zebrafish *rpl36* (ENSDARG00000100588) and *rps20* (ENSDART00000052331.6) were amplified by RT-PCR and cloned into pCS2+ via EcoRI/XhoI restriction sites using a DNA Ligation Kit (Takara). The ORF of zebrafish *znf598* (ENSDARG00000014945) was amplified by RT-PCR and cloned into pCS2+ via XhoI/XbaI restriction sites using a DNA Ligation Kit (Takara). To generate *znf598* point mutation in ORF (*znf598* C13/16A), WT ORF was amplified using point mutated primers and cloned into pCS2+ via XhoI/XbaI restriction sites using a DNA Ligation Kit (Takara). The ORFs of zebrafish *etf1b* (ENSDARG00000043976), *rps10* (ENSDARG00000034897), *rps3* (ENSDART00000185844.1), and *rps2* (ENSDART00000138107.3) were amplified by RT-PCR and cloned into pCS2 + HA using NEBuilder HiFi DNA Assembly (New England Biolabs). The pCS2 + HA was generated by inserting synthetic DNA fragments with HA-tag sequence into pCS2+ via EcoRI/XbaI restriction sites. To generate *etf1b* and *rps10* point mutations in ORFs (*etf1b*-AAQ, *rps10*-K139R, *rps10*-K140R, and *rps10*-K139/140R), WT ORFs were amplified using point mutated primers. DNA fragments were then assembled using NEBuilder HiFi DNA Assembly (New England Biolabs).

Polysome analysis

For polysome analysis, we followed the original protocol with some modifications (Mishima et al. 2012). Zebrafish embryos at 24 hpf were dechorionated with 1 mg/mL Pronase (Sigma). Sixty dechorionated embryos were homogenized in buffer A (20 mM HEPES-KOH pH 7.5, 100 mM KCl, 10 mM $MgCl_2$, 0.25% NP-40, 250 mM sucrose, 2 mM DTT, 10 µg/mL CHX, 100 U/mL RNase inhibitor [Promega], Complete Protease Inhibitor EDTA-free in nuclease-free water). Lysates were incubated for 5 min on ice and centrifuged for 5 min at 12,000 rpm at 4°C. Clarified lysates were loaded onto a continuous 10%–45% (*w/v*) sucrose gradient prepared in buffer B (20 mM HEPES-KOH pH 7.5, 100 mM KCl, 10 mM $MgCl_2$, 2 mM DTT, 10 µg/mL CHX, 100 U/mL RNase inhibitor [Takara]). Gradients were centrifuged in a P40ST rotor (Himac) for 180 min at 36,000 rpm at 4°C. Polysome gradients were analyzed using a gradient station (BioComp) coupled to a Triax Flow Cell detector (FC-2). Each fraction was collected and precipitated by ethanol (75% final). Pellets were dissolved in Sample Buffer Solution (Fujifilm-Wako). Samples were incubated for 30 min at 92°C and proceeded to SDS–PAGE followed by immunoblotting analysis.

Immunoblotting analysis

Samples were incubated with Sample Buffer Solution (Fujifilm-Wako) for 10 min at 92°C. The SDS–PAGE and immunoblotting experiments were carried out according to standard protocols. Signals were developed using ImmunoStar LD (Fujifilm-Wako) or Luminata Forte (Millipore) and detected using an Amersham Imager 680 (GE Healthcare). Antibodies used in this study are shown in Supplemental Table S4.

Immunoprecipitation

To conduct the immunoprecipitation assay, we followed the original protocol with some modifications (Simsek et al. 2017). For immunoprecipitation by an anti-FLAG antibody, 15–45 zebrafish embryos were homogenized in lysis buffer A (25 mM Tris-HCl pH 7.6, 150 mM NaCl, 15 mM $MgCl_2$, 1 mM DTT, 8% glycerol, 1% triton X-100, 50 µM PR-619, 100 U/mL RNase inhibitor [Takara], Complete Protease Inhibitor EDTA-free in nuclease-free water). Lysates were incubated for 5 min on ice and centrifuged for 5 min at 2000*g* at 4°C. Supernatants were incubated with Anti-DYKDDDDK tag Antibody Beads (Fujifilm-Wako) for 15 min on rotation at 4°C.

Anti-DYKDDDDK tag Antibody Beads were prepared by washing with wash buffer (25 mM Tris-HCl pH 7.6, 150 mM NaCl, 15 mM $MgCl_2$, 1 mM DTT, 8% glycerol, 1% triton X-100) three times. Four microliters of slurry beads were used per embryo.

After 15 min incubation at 4°C with rotation, beads were washed twice with buffer B (25 mM Tris-HCl pH 7.6, 150 mM NaCl, 15 mM $MgCl_2$, 1 mM DTT, 1% triton X-100, 50 µM PR-619) and once with buffer C (25 mM Tris-HCl pH 7.6, 150 mM NaCl, 15 mM $MgCl_2$, 1% triton X-100, 50 µM PR-619). Samples were eluted from the beads by incubating with 0.5 mg/mL FLAG peptide (Medical & Biological Laboratories Co., Ltd.) in buffer C at 25°C for 30 min.

For EDTA-treated samples (related to Fig. 3C,D), 50 mM EDTA was used in place of 15 mM $MgCl_2$ in buffers A, B, C, and wash buffer. For post-purification EDTA-treated samples (related to Supplemental Fig. S3C), FLAG-IPs obtained in the EDTA-free

conditions were separated and incubated continuously with or without 50 mM EDTA for 25 min at 4°C and for 30 min at 25°C.

For mass spectrometry analysis, beads were washed twice using buffer D (25 mM Tris-HCl pH 7.6, 150 mM NaCl, 15 mM $MgCl_2$) after washing with buffer B. We followed the original protocol (Imami et al. 2018, 2023) with some modifications. Beads were resuspended in PTS buffer (12 mM sodium deoxycholate [SDC] , 12 mM sodium *N*-lauroylsarcosinate [SLS] in 100 mM Tris-HCl pH 8.0) followed by incubation for 30 min at 37°C under constant agitation. After the incubation, the supernatant was reduced with 10 mM dithiothreitol (DTT) at 37°C for 30 min and alkylated with 50 mM iodoacetamide (IAA) at room temperature for 30 min in a dark room. The samples were diluted five times with 50 mM ammonium bicarbonate (ABC). For Supplemental Figure S2A,B and Supplemental Table S1, proteins were digested by 0.5 µg lysyl endopeptidase (LysC) (Fujifilm-Wako) and 0.5 µg Trypsin (Promega) at room temperature overnight. For Figure 4E,F, proteins were digested by LysC, Trypsin, or Glu-C (Promega). The next day, 500 µL ethyl acetate (Fujifilm-Wako) was added to the sample, and digestion was quenched by adding 0.5% trifluoroacetic acid (TFA) (final concentration). The samples were shaken for 1 min and centrifugated at 15,000*g* for 2 min at room temperature. The organic phase containing SDC and SLS was discarded. The resulting peptide solution was evaporated in a SpeedVac. The residue was resuspended in 0.1% TFA and desalted with SDB-XC Stage tips (Rappsilber et al. 2007) prior to LC–MS/MS analysis.

For high-salt washes experiments (related to Supplemental Fig. S3A,B), after 15 min incubation at 4°C rotation, beads were washed twice with buffer B containing 400 mM NaCl (25 mM Tris-HCl pH 7.6, 400 mM NaCl, 15 mM $MgCl_2$, 1 mM DTT, 1% triton X-100, 50 µM PR-619). Afterward, beads were washed once with buffer C containing 400 mM NaCl (25 mM Tris-HCl pH 7.6, 400 mM NaCl, 15 mM $MgCl_2$, 1% triton X-100, 50 µM PR-619). Samples were then eluted off the beads using 0.5 mg/mL FLAG peptide in buffer C containing 400 mM NaCl for 30 min at 25°C. RNA was extracted from a portion of the samples, and rRNAs were quantified by agarose gel electrophoresis, to compensate for differences in the quantities of ribosomes recovered from low and high-salt conditions. The equal amounts of ribosomes estimated from the RNA analysis were subjected to immunoblotting analysis and protein staining.

LC–MS/MS analysis

Nanoscale reversed-phase liquid chromatography coupled with tandem mass spectrometry (nanoLC/MS/MS) was performed on an Orbitrap Exploris 480 (related to Supplemental Fig. S2A,B and Supplemental Table S1) or an Orbitrap Fusion Lumos mass spectrometer (related to Fig. 4E,F) (Thermo Fisher Scientific) connected to a Thermo Ultimate 3000 RSLCnano pump equipped with a self-pulled analytical column (150 mm length × 100 µm i.d.) (Ishihama et al. 2002) packed with ReproSil-Pur C18-AQ materials (3 µm or 1.9 µm; Dr. Maisch GmbH). The mobile phases comprised (A) 0.5% acetic acid and (B) 0.5% acetic acid and 80% ACN.

For the Orbitrap Exploris 480 system (related to Supplemental Fig. S2A,B and Supplemental Table S1), peptides were separated on self-pulled needle columns (250 mm, 100 µm ID) packed with Reprosil-Pur 120 C18-AQ1.9 µm at 50°C in a column oven. The flow rate was 400 nL/min. The flow gradient was set as follows: 5% B in 5 min, 5%–19% B in 55.3 min, 19%–29% B in 21 min, 29%–40% B in 8.7 min, and 40%–99% B in 0.1 min, followed by 99% B for 4.9 min. The electrospray voltage was set to 2.2 kV in the positive mode. The mass spectrometric analysis was carried out with the FAIMS Pro Interface (Thermo Fisher Scientific). The compensation voltage (CV) was set to −40, −60, and −80 and the cycle time of each CV experiment was set to 1 sec. The mass range of the survey scan was from 375 to 1500 *m/z* with a resolution of 60,000, 300% normalized automatic gain control (AGC) target and auto maximum injection time. The first mass of the MS/MS scan was set to 120 *m/z* with a resolution of 15,000, standard AGC, and auto maximum injection time. Fragmentation was performed by HCD with a normalized collision energy of 30%. The dynamic exclusion time was set to 20 sec.

The Orbitrap Fusion Lumos instrument was operated in the data-dependent mode with a full scan in the Orbitrap followed by MS/MS scans using HCD (related to Fig. 4E,F). Peptides were eluted from the analytical column at a flow rate of 500 nL/min, with the following gradient: 5%–10% B for 5 min, 10%–40% B for 60 min, 40%–99% B for 5 min, and 99% for 5 min. The applied voltage for ionization was 2.4 kV. The full scans were performed with a resolution of 120,000, the standard AGC target mode, and a maximum injection time of 50 msec. The MS scan range was *m/z* 300–1500. The CV of the FAIMS Pro Interface was set to −40, −60, and −80, and the cycle time of each CV experiment was set to 1 sec. The MS/MS scans were collected in the ion trap with the rapid mode, the standard AGC target mode, and a maximum injection time of 35 msec. The isolation window was set to 1.6, and the normalized HCD collision energy was 30. Dynamic exclusion was applied for 20 sec.

Processing of proteome data

All raw data files were analyzed and processed by maxquant (version 1.6.15.0 or 1.6.17.0) (Cox and Mann 2008), and the database search was performed with Andromeda (Cox et al. 2011), which is a peptide search engine integrated into the MaxQuant environment. Searches were conducted against a zebrafish UniProt database (version 2021-3; 46,849 protein entries) spiked with common contaminants and enzyme sequences. Search parameters included two missed cleavage sites and variable modifications such as methionine oxidation; protein amino-terminal acetylation; deamidation of glutamine and asparagine residues; and di-glycine of lysine residue (only ubiquitination analysis related to Fig. 4E,F). Cysteine carbamidomethylation was set as a fixed modification. The enzyme was set as trypsin/P, which also cleaves at the carboxyl side of the amino acids lysine or arginine, also if a proline follows, lysC (cleaves after lysine), or Glu-C (cleaves after glutamic acid). The peptide mass tolerance was 4.5 ppm, and the MS/MS tolerance was 20 ppm. The false discovery rate (FDR) was set to 1% at the peptide spectrum match level and protein level. The "match between runs" function was performed. All necessary information regarding proteomic analyses, including protein and peptide lists, was deposited in a publicly accessible repository (jPOST) (Okuda et al. 2017; Moriya et al. 2019) with the data set identifier, PXD039560.

Microinjection

Microinjection was performed as described in Mishima and Tomari (2016) using an IM300 Microinjector (Narishige).

Approximately 1000 pL of the solution was injected per embryo within 15 min after spawning. Embryos were developed in system water at 28.5°C.

Protein staining

Following SDS–PAGE, the gel was immersed in Oriole solution (Bio-Rad) for 90 min while being constantly agitated. For 5 min, the gel was rinsed twice with distilled water. Amersham Imager 680 was used to detect the signals (GE Healthcare).

RNA extraction

RNA samples were extracted from zebrafish embryos or FLAG-IPs using TRI Reagent (Molecular Research Center). Ethachinmate (Nippon gene) was used in ethanol precipitation to recover a small quantity of RNA.

In vitro mRNA transcription

mRNA was synthesized from a linearized plasmid DNA template using the SP6 Scribe Standard RNA IVT Kit and the ScriptCap m7G Capping System (Cellscript) or mMessage mMachine SP6 (Thermo Fisher Scientific), followed by purification with the RNeasy Mini Kit (Qiagen).

Harringtonine and cycloheximide treatment

Embryos were incubated with the drugs at the indicated concentrations and duration at 28.5°. Twenty-three-hour post-fertilization embryos were given an hour of treatment with HTN (LKT Laboratories, Inc.) at concentrations of 50, 100, 200, or 400 µg/mL. Twenty-two-hour post-fertilization embryos were given 2 h of treatment with CHX (Fujifilm-Wako) at concentrations of 1.25, 5, 20, 80, 320, or 1280 µg/mL.

Quantification of ubiquitination signals

Signals were quantified using the ROI manager function of the ImageJ software (http://imageJ.nih.gov/ij/). The background signal was measured with the empty lane and subtracted from quantified values. Relative ubiquitination levels were calculated by dividing a ubiquitin signal by a corresponding protein staining signal. Three biological replicates were used in the experiments, and averages were computed.

SUPPLEMENTAL MATERIAL

Supplemental material is available for this article.

ACKNOWLEDGMENTS

The authors thank our laboratory members for discussions and technical assistance, especially Kimi Wakabayashi for fish maintenance. We thank Toshifumi Inada for technical advice on the ribosome analysis. This work was supported by the Japan Society for the Promotion of Science (JSPS) (JP18H02370 and JP22K19300) and the Japan Agency for Medical Research and Development (AMED) (AMED PRIME, JP20gm6310017) to Y.M. Additional support was provided by JSPS (20H03241 and 21H05720) and the Japan Science and Technology Agency (JST) FOREST (JPMJFR214L) to K.I., JST ACT X (JP1159335) to H.T., JSPS (JP21H02459) to Y.I., and MEXT Grants-in-Aid for Scientific Research (20H05926, 21K06053) and a grant from the Institute for Fermentation, Osaka (G-2021-2-063) to S.C. N.U. was a recipient of the Support for Pioneering Research Initiated by the Next Generation (SPRING) program by JST (JPMJSP2157).

Author contributions: N.U. and Y.M. designed the project. N.U. performed the experiments under the supervision of Y.M., K.I., H. T., and S.C. K.I. and Y.I. performed the mass spectrometry analysis. N.U. and Y.M. analyzed the data and drafted the manuscript. All the authors discussed the results and approved the manuscript for submission.

Received February 12, 2023; accepted September 5, 2023.

REFERENCES

Back S, Gorman AW, Vogel C, Silva GM. 2019. Site-specific K63 ubiquitinomics provides insights into translation regulation under stress. *J Proteome Res* **18:** 309–318. doi:10.1021/acs.jproteome.8b00623

Bashan A, Yonath A. 2008. Correlating ribosome function with high-resolution structures. *Trends Microbiol* **16:** 326–335. doi:10.1016/j.tim.2008.05.001

Bengtson MH, Joazeiro CAP. 2010. Role of a ribosome-associated E3 ubiquitin ligase in protein quality control. *Nature* **467:** 470–473. doi:10.1038/nature09371

Brandman O, Stewart-Ornstein J, Wong D, Larson A, Williams CC, Li GW, Zhou S, King D, Shen PS, Weibezahn J, et al. 2012. A ribosome-bound quality control complex triggers degradation of nascent peptides and signals translation stress. *Cell* **151:** 1042–1054. doi:10.1016/j.cell.2012.10.044

Cox J, Mann M. 2008. MaxQuant enables high peptide identification rates, individualized p.p.b.-range mass accuracies and proteome-wide protein quantification. *Nat Biotechnol* **26:** 1367–1372. doi:10.1038/nbt.1511

Cox J, Neuhauser N, Michalski A, Scheltema RA, Olsen JV, Mann M. 2011. Andromeda: a peptide search engine integrated into the MaxQuant environment. *J Proteome Res* **10:** 1794–1805. doi:10.1021/pr101065j

Dalla Venezia N, Vincent A, Marcel V, Catez F, Diaz JJ. 2019. Emerging role of eukaryote ribosomes in translational control. *Int J Mol Sci* **20:** 1226. doi:10.3390/ijms20051226

De La Cruz J, Karbstein K, Woolford JL. 2015. Functions of ribosomal proteins in assembly of eukaryotic ribosomes *in vivo*. *Annu Rev Biochem* **84:** 93–129. doi:10.1146/annurev-biochem-060614-033917

D'Orazio KN, Wu CCC, Sinha N, Loll-Krippleber R, Brown GW, Green R. 2019. The endonuclease Cue2 cleaves mRNAs at stalled ribosomes during no go decay. *Elife* **8:** e49117. doi: 10.7554/eLife.49117

Emmott E, Jovanovic M, Slavov N. 2019. Ribosome stoichiometry: from form to function. *Trends Biochem Sci* **44:** 95–109. doi:10.1016/j.tibs.2018.10.009

Garshott DM, Sundaramoorthy E, Leonard M, Bennett EJ. 2020. Distinct regulatory ribosomal ubiquitylation events are reversible and hierarchically organized. *Elife* **9:** e54023. doi:10.7554/eLife.54023

Garshott DM, An H, Sundaramoorthy E, Leonard M, Vicary A, Harper JW, Bennett EJ. 2021. iRQC, a surveillance pathway for 40S ribosomal quality control during mRNA translation initiation. *Cell Rep* **36:** 109642. doi:10.1016/j.celrep.2021.109642

Garzia A, Jafarnejad SM, Meyer C, Chapat C, Gogakos T, Morozov P, Amiri M, Shapiro M, Molina H, Tuschl T, et al. 2017. The E3 ubiquitin ligase and RNA-binding protein ZNF598 orchestrates ribosome quality control of premature polyadenylated mRNAs. *Nat Commun* **8:** 16056. doi:10.1038/ncomms16056

Garzia A, Meyer C, Tuschl T. 2021. The E3 ubiquitin ligase RNF10 modifies 40S ribosomal subunits of ribosomes compromised in translation. *Cell Rep* **36:** 109468. doi:10.1016/j.celrep.2021.109468

Glover ML, Burroughs AM, Monem PC, Egelhofer TA, Pule MN, Aravind L, Arribere JA. 2020. NONU-1 encodes a conserved endonuclease required for mRNA translation surveillance. *Cell Rep* **30:** 4321–4331.e4. doi:10.1016/j.celrep.2020.03.023

Han P, Shichino Y, Schneider-Poetsch T, Mito M, Hashimoto S, Udagawa T, Kohno K, Yoshida M, Mishima Y, Inada T, et al. 2020. Genome-wide survey of ribosome collision. *Cell Rep* **31:** 107610. doi:10.1016/j.celrep.2020.107610

Higgins R, Gendron JM, Rising L, Mak R, Webb K, Kaiser SE, Zuzow N, Riviere P, Yang B, Fenech E, et al. 2015. The unfolded protein response triggers site-specific regulatory ubiquitylation of 40S ribosomal proteins. *Mol Cell* **59:** 35–49. doi:10.1016/j.molcel.2015.04.026

Ikeuchi K, Tesina P, Matsuo Y, Sugiyama T, Cheng J, Saeki Y, Tanaka K, Becker T, Beckmann R, Inada T. 2019. Collided ribosomes form a unique structural interface to induce Hel2-driven quality control pathways. *EMBO J* **38:** e100276. doi:10.15252/embj.2018100276

Imami K, Milek M, Bogdanow B, Yasuda T, Kastelic N, Zauber H, Ishihama Y, Landthaler M, Selbach M. 2018. Phosphorylation of the ribosomal protein RPL12/uL11 affects translation during mitosis. *Mol Cell* **72:** 84–98.e9. doi:10.1016/j.molcel.2018.08.019

Imami K, Selbach M, Ishihama Y. 2023. Monitoring mitochondrial translation by pulse SILAC. *J Biol Chem* **299:** 102865. doi:10.1016/j.jbc.2022.102865

Inada T. 2020. Quality controls induced by aberrant translation. *Nucleic Acids Res* **48:** 1084–1096. doi:10.1093/nar/gkz1201

Inada T, Winstall E, Tarun SZ, Yates JR, Schieltz D, Sachs AB. 2002. One-step affinity purification of the yeast ribosome and its associated proteins and mRNAs. *RNA* **8:** 948–958. doi:10.1017/S1355838202026018

Ishihama Y, Rappsilber J, Andersen JS, Mann M. 2002. Microcolumns with self-assembled particle frits for proteomics. *J Chromatogr A* **979:** 233–239. doi:10.1016/S0021-9673(02)01402-4

Ishimura R, Nagy G, Dotu I, Zhou H, Yang XL, Schimmel P, Senju S, Nishimura Y, Chuang JH, Ackerman SL. 2014. Ribosome stalling induced by mutation of a CNS-specific tRNA causes neurodegeneration. *Science* **345:** 455–459. doi:10.1126/science.1249749

Joazeiro CAP. 2017. Ribosomal stalling during translation: providing substrates for ribosome-associated protein quality control. *Annu Rev Cell Dev Biol* **33:** 343–368. doi:10.1146/annurev-cellbio-111315-125249

Joazeiro CAP. 2019. Mechanisms and functions of ribosome-associated protein quality control. *Nat Rev Mol Cell Biol* **20:** 368–383. doi:10.1038/s41580-019-0118-2

Johannes G, Carter MS, Eisen MB, Brown PO, Sarnow P. 1999. Identification of eukaryotic mRNAs that are translated at reduced cap binding complex eIF4F concentrations using a cDNA microarray. *Proc Natl Acad Sci* **96:** 13118–13123. doi:10.1073/pnas.96.23.13118

Juszkiewicz S, Hegde RS. 2017. Initiation of quality control during poly(A) translation requires site-specific ribosome ubiquitination. *Mol Cell* **65:** 743–750.e4. doi:10.1016/j.molcel.2016.11.039

Juszkiewicz S, Chandrasekaran V, Lin Z, Kraatz S, Ramakrishnan V, Hegde RS. 2018. ZNF598 is a quality control sensor of collided ribosomes. *Mol Cell* **72:** 469–481.e7. doi:10.1016/j.molcel.2018.08.037

Juszkiewicz S, Slodkowicz G, Lin Z, Freire-Pritchett P, Peak-Chew S-Y, Hegde RS. 2020a. Ribosome collisions trigger *cis*-acting feedback inhibition of translation initiation. *Elife* **9:** e60038. doi:10.7554/eLife.60038

Juszkiewicz S, Speldewinde SH, Wan L, Svejstrup JQ, Hegde RS. 2020b. The ASC-1 complex disassembles collided ribosomes. *Mol Cell* **79:** 603–614.e8. doi:10.1016/j.molcel.2020.06.006

Leesch F, Lorenzo-Orts L, Pribitzer C, Grishkovskaya I, Roehsner J, Chugunova A, Matzinger M, Roitinger E, Belačić K, Kandolf S, et al. 2023. A molecular network of conserved factors keeps ribosomes dormant in the egg. *Nature* **613:** 712–720. doi:10.1038/s41586-022-05623-y

Li D, Wang J. 2020. Ribosome heterogeneity in stem cells and development. *J Cell Biol* **219:** e202001108. doi:10.1083/jcb.202001108

Li S, Ikeuchi K, Kato M, Buschauer R, Sugiyama T, Adachi S, Kusano H, Natsume T, Berninghausen O, Matsuo Y, et al. 2022. Sensing of individual stalled 80S ribosomes by Fap1 for nonfunctional rRNA turnover. *Mol Cell* **82:** 3424–3437.e8. doi:10.1016/j.molcel.2022.08.018

Małecki JM, Odonohue MF, Kim Y, Jakobsson ME, Gessa L, Pinto R, Wu J, Davydova E, Moen A, Olsen JV, et al. 2021. Human METTL18 is a histidine-specific methyltransferase that targets RPL3 and affects ribosome biogenesis and function. *Nucleic Acids Res* **49:** 3185–3203. doi:10.1093/nar/gkab088

Martin I, Kim JW, Lee BD, Kang HC, Xu JC, Jia H, Stankowski J, Kim MS, Zhong J, Kumar M, et al. 2014. Ribosomal protein s15 phosphorylation mediates LRRK2 neurodegeneration in Parkinson's disease. *Cell* **157:** 472–485. doi:10.1016/j.cell.2014.01.064

Martini OHW, Gould HJ. 1975. Molecular weight distribution of ribosomal proteins from several vertebrate species. *Mol Gen Genet* **142:** 317–331. doi:10.1007/BF00271255

Matsuki Y, Matsuo Y, Nakano Y, Iwasaki S, Yoko H, Udagawa T, Li S, Saeki Y, Yoshihisa T, Tanaka K, et al. 2020. Ribosomal protein S7 ubiquitination during ER stress in yeast is associated with selective mRNA translation and stress outcome. *Sci Rep* **10:** 19669. doi:10.1038/s41598-020-76239-3

Matsuo Y, Ikeuchi K, Saeki Y, Iwasaki S, Schmidt C, Udagawa T, Sato F, Tsuchiya H, Becker T, Tanaka K, et al. 2017. Ubiquitination of stalled ribosome triggers ribosome-associated quality control. *Nat Commun* **8:** 159. doi:10.1038/s41467-017-00188-1

Matsuo Y, Tesina P, Nakajima S, Mizuno M, Endo A, Buschauer R, Cheng J, Shounai O, Ikeuchi K, Saeki Y, et al. 2020. RQT complex dissociates ribosomes collided on endogenous RQC substrate SDD1. *Nat Struct Mol Biol* **27:** 323–332. doi:10.1038/s41594-020-0393-9

Matsuura-Suzuki E, Shimazu T, Takahashi M, Kotoshiba K, Suzuki T, Kashiwagi K, Sohtome Y, Akakabe M, Sodeoka M, Dohmae N, et al. 2022. METTL18-mediated histidine methylation of RPL3 modulates translation elongation for proteostasis maintenance. *Elife* **11:** e72780. doi:10.7554/eLife.72780

Meyer C, Garzia A, Morozov P, Molina H, Tuschl T. 2020. The G3BP1-family-USP10 deubiquitinase complex rescues ubiquitinated 40S subunits of ribosomes stalled in translation from lysosomal degradation. *Mol Cell* **77:** 1193–1205.e5. doi:10.1016/j.molcel.2019.12.024

Mishima Y, Tomari Y. 2016. Codon usage and 3′ UTR length determine maternal mRNA stability in zebrafish. *Mol Cell* **61:** 874–885. doi:10.1016/j.molcel.2016.02.027

Mishima Y, Fukao A, Kishimoto T, Sakamoto H, Fujiwara T, Inoue K. 2012. Translational inhibition by deadenylation-independent mechanisms is central to microRNA-mediated silencing in zebrafish. *Proc Natl Acad Sci* **109:** 1104–1109. doi:10.1073/pnas.1113350109

Mishima Y, Han P, Ishibashi K, Kimura S, Iwasaki S. 2022. Ribosome slowdown triggers codon-mediated mRNA decay independently

of ribosome quality control. *EMBO J* **41:** e109256. doi:10.15252/embj.2021109256
Moriya Y, Kawano S, Okuda S, Watanabe Y, Matsumoto M, Takami T, Kobayashi D, Yamanouchi Y, Araki N, Yoshizawa AC, et al. 2019. The jPOST environment: an integrated proteomics data repository and database. *Nucleic Acids Res* **47:** D1218–D1224. doi:10.1093/nar/gky899
Narita M, Denk T, Matsuo Y, Sugiyama T, Kikuguchi C, Ito S, Sato N, Suzuki T, Hashimoto S, Machová I, et al. 2022. A distinct mammalian disome collision interface harbors K63-linked polyubiquitination of uS10 to trigger hRQT-mediated subunit dissociation. *Nat Commun* **13:** 6411. doi:10.1038/s41467-022-34097-9
Okuda S, Watanabe Y, Moriya Y, Kawano S, Yamamoto T, Matsumoto M, Takami T, Kobayashi D, Araki N, Yoshizawa AC, et al. 2017. jPOSTrepo: an international standard data repository for proteomes. *Nucleic Acids Res* **45:** D1107–D1111. doi:10.1093/nar/gkw1080
Oltion K, Carelli JD, Yang T, See SK, Wang H-Y, Kampmann M, Taunton J. 2023. An E3 ligase network engages GCN1 to promote the degradation of translation factors on stalled ribosomes. *Cell* **186:** 346–362.e17. doi:10.1016/j.cell.2022.12.025
Panasenko OO, Collart MA. 2012. Presence of Not5 and ubiquitinated Rps7A in polysome fractions depends upon the Not4 E3 ligase. *Mol Microbiol* **83:** 640–653. doi:10.1111/j.1365-2958.2011.07957.x
Pochopien AA, Beckert B, Kasvandik S, Berninghausen O, Beckmann R, Tenson T, Wilson DN. 2021. Structure of Gcn1 bound to stalled and colliding 80S ribosomes. *Proc Natl Acad Sci* **118:** e2022756118. doi:10.1073/pnas.2022756118
Rappsilber J, Mann M, Ishihama Y. 2007. Protocol for micro-purification, enrichment, pre-fractionation and storage of peptides for proteomics using StageTips. *Nat Protoc* **2:** 1896–1906. doi:10.1038/nprot.2007.261
Reschke M, Clohessy JG, Seitzer N, Goldstein DP, Breitkopf SB, Schmolze DB, Ala U, Asara JM, Beck AH, Pandolfi PP. 2013. Characterization and analysis of the composition and dynamics of the mammalian riboproteome. *Cell Rep* **4:** 1276–1287. doi:10.1016/j.celrep.2013.08.014
Sanz E, Yang L, Su T, Morris DR, McKnight GS, Amieux PS. 2009. Cell-type-specific isolation of ribosome-associated mRNA from complex tissues. *Proc Natl Acad Sci* **106:** 13939–13944. doi:10.1073/pnas.0907143106
Schuller AP, Wu CCC, Dever TE, Buskirk AR, Green R. 2017. eIF5A functions globally in translation elongation and termination. *Mol Cell* **66:** 194–205.e5. doi:10.1016/j.molcel.2017.03.003
Shao S, Hegde RS. 2014. Reconstitution of a minimal ribosome-associated ubiquitination pathway with purified factors. *Mol Cell* **55:** 880–890. doi:10.1016/j.molcel.2014.07.006
Shi Z, Fujii K, Kovary KM, Genuth NR, Röst HL, Teruel MN, Barna M. 2017. Heterogeneous ribosomes preferentially translate distinct subpools of mRNAs genome-wide. *Mol Cell* **67:** 71–83.e7. doi:10.1016/j.molcel.2017.05.021
Silva GM, Finley D, Vogel C. 2015. K63 polyubiquitination is a new modulator of the oxidative stress response. *Nat Struct Mol Biol* **22:** 116–123. doi:10.1038/nsmb.2955
Simms CL, Yan LL, Zaher HS, Simms CL, Yan LL, Zaher HS. 2017. Ribosome collision is critical for quality control during no-go decay. *Mol Cell* **68:** 361–373.e5. doi:10.1016/j.molcel.2017.08.019
Simsek D, Barna M. 2017. An emerging role for the ribosome as a nexus for post-translational modifications. *Curr Opin Cell Biol* **45:** 92–101. doi:10.1016/j.ceb.2017.02.010
Simsek D, Tiu GC, Flynn RA, Byeon GW, Leppek K, Xu AF, Chang HY, Barna M. 2017. The mammalian ribo-interactome reveals ribosome functional diversity and heterogeneity. *Cell* **169:** 1051–1065.e18. doi:10.1016/j.cell.2017.05.022
Sitron CS, Park JH, Brandman O. 2017. Asc1, Hel2, and Slh1 couple translation arrest to nascent chain degradation. *RNA* **23:** 798–810. doi:10.1261/rna.060897.117
Snaurova R, Vdovin A, Durech M, Nezval J, Zihala D, Jelinek T, Hajek R, Simicek M. 2022. Deubiquitinase OTUD1 resolves stalled translation on polyA and rare codon rich mRNAs. *Mol Cell Biol* **42:** e0026522. doi:10.1128/mcb.00265-22
Spence J, Gali RR, Dittmar G, Sherman F, Karin M, Finley D. 2000. Cell cycle-regulated modification of the ribosome by a variant multiubiquitin chain. *Cell* **102:** 67–76. doi:10.1016/S0092-8674(00)00011-8
Sugiyama T, Li S, Kato M, Ikeuchi K, Ichimura A, Matsuo Y, Inada T. 2019. Sequential ubiquitination of ribosomal protein uS3 triggers the degradation of non-functional 18S rRNA. *Cell Rep* **26:** 3400–3415.e7. doi:10.1016/j.celrep.2019.02.067
Sundaramoorthy E, Leonard M, Mak R, Liao J, Fulzele A, Bennett EJ. 2017. ZNF598 and RACK1 regulate mammalian ribosome-associated quality control function by mediating regulatory 40S ribosomal ubiquitylation. *Mol Cell* **65:** 751–760.e4. doi:10.1016/j.molcel.2016.12.026
Takehara Y, Yashiroda H, Matsuo Y, Zhao X, Kamigaki A, Matsuzaki T, Kosako H, Inada T, Murata S. 2021. The ubiquitination-deubiquitination cycle on the ribosomal protein eS7A is crucial for efficient translation. *iScience* **24:** 102145. doi:10.1016/j.isci.2021.102145
Tryon RC, Pisat N, Johnson SL, Dougherty JD. 2013. Development of translating ribosome affinity purification for zebrafish. *Genesis* **51:** 187–192. doi:10.1002/dvg.22363
Vejnar CE, Moreno-Mateos MA, Cifuentes D, Bazzini AA, Giraldez AJ. 2016. Optimization strategies for the CRISPR-Cas9 genome-editing system. *Cold Spring Harb Protoc* **2016:** 829–832. doi:10.1101/pdb.top090894
Vind AC, Snieckute G, Blasius M, Tiedje C, Krogh N, Bekker-Jensen DB, Andersen KL, Nordgaard C, Tollenaere MAX, Lund AH, et al. 2020. ZAKα recognizes stalled ribosomes through partially redundant sensor domains. *Mol Cell* **78:** 700–713. doi:10.1016/j.molcel.2020.03.021
Walczak CP, Leto DE, Zhang L, Riepe C, Muller RY, DaRosa PA, Ingolia NT, Elias JE, Kopito RR. 2019. Ribosomal protein RPL26 is the principal target of UFMylation. *Proc Natl Acad Sci* **116:** 1299–1308. doi:10.1073/pnas.1816202116
Wang L, Xu Y, Rogers H, Saidi L, Noguchi CT, Li H, Yewdell JW, Guydosh NR, Ye Y. 2020. UFMylation of RPL26 links translocation-associated quality control to endoplasmic reticulum protein homeostasis. *Cell Res* **30:** 5–20. doi:10.1038/s41422-019-0236-6
Wu CC-C, Peterson A, Zinshteyn B, Regot S, Green R. 2020. Ribosome collisions trigger general stress responses to regulate cell fate. *Cell* **182:** 404–416.e14. doi:10.1016/j.cell.2020.05.008
Xue S, Barna M. 2012. Specialized ribosomes: a new frontier in gene regulation and organismal biology. *Nat Rev Mol Cell Biol* **23:** 355–369. doi:10.1038/nrm3359
Yan LL, Zaher HS. 2021. Ribosome quality control antagonizes the activation of the integrated stress response on colliding ribosomes. *Mol Cell* **81:** 614–628.e4. doi:10.1016/j.molcel.2020.11.033
Zhang BQ, Chen ZQ, Dong YQ, You D, Zhou Y, Ye BC. 2022. Selective recruitment of stress-responsive mRNAs to ribosomes for translation by acetylated protein S1 during nutrient stress in *Escherichia coli*. *Commun Biol* **5:** 892. doi:10.1038/s42003-022-03853-4

See the following page for ***Meet the First Author***

MEET THE FIRST AUTHOR

Nozomi Ugajin

***Meet the First Author(s)* is an editorial feature within *RNA*, in which the first author(s) of research-based papers in each issue have the opportunity to introduce themselves and their work to readers of *RNA* and the RNA research community. Nozomi Ugajin is the first author of this paper, "Znf598-mediated Rps10/eS10 ubiquitination contributes to the ribosome ubiquitination dynamics during zebrafish development." She is a PhD student in Kyoto Sangyo University, where she is studying ribosome ubiquitination.**

What are the major results described in your paper and how do they impact this branch of the field?

We showed that ribosome ubiquitination levels dynamically change during zebrafish development. In particular, our results demonstrated that Rps10/eS10 ubiquitination plays an important role in forming the ribosome ubiquitination pattern directly and indirectly. Our study will assist in expanding the ribosome ubiquitination field in multicellular organisms.

What led you to study RNA or this aspect of RNA science?

I was fascinated by the morphological dynamic changes during embryogenesis when I was in high school, therefore I wanted to reveal the molecular mechanism underlying embryogenesis. The molecular mechanisms underlying translational activation and degradation of maternal mRNA are interesting processes for me and they immersed me in RNA science.

During the course of these experiments, were there any surprising results or particular difficulties that altered your thinking and subsequent focus?

Due to the low ubiquitination level on ribosomes, we failed to identify ubiquitinated ribosomal proteins by mass spectrometry analysis using FLAG-immunoprecipitants from differential developmental stages' embryos. We altered our approach from identifying ubiquitinated proteins to identifying a ubiquitin ligase that contributes to forming the ribosome ubiquitination pattern. As a result, to identify ubiquitinated ribosomal proteins, we performed mass spectrometry analysis using Znf598-overexpressed embryos.

What are some of the landmark moments that provoked your interest in science or your development as a scientist?

When I was a high school student, my biology teacher invited me to a science club that was supported by the Ministry of Education, Culture, Sports, Science and Technology in Japan. Through the club, I went to several universities and participated in science lectures there. That was definitely my landmark moment that started my life with science.

If you were able to give one piece of advice to your younger self, what would that be?

Because I'm not skilled at English, it was very challenging for me to write the manuscript in English. So, I would tell my younger self to study English hard.

Are there specific individuals or groups who have influenced your philosophy or approach to science?

Dr. Koshi Imami, who is one of my coauthors, has influenced my scientific philosophy. He continuously develops original cutting-edge proteomic technologies, and by using these systems, he and his laboratory expand insightful research. I respect and admire his initiative in science.

What are your subsequent near- or long-term career plans?

I'm going to work at a pharmaceutical company as a researcher in Japan after graduation. I will shift my research subject and contribute to human health care.